ABMP16 PDF fit: low x, large x and higher-twist effects

S.Alekhin (*Univ. of Hamburg & IHEP Protvino)*

sa, Blümlein, Moch, Plačakytė PRD 96, 014011 (2017)
sa, Blümlein, Moch PLB 777, 134 (2018)
sa, Blümlein, Moch EPJC 78, 477 (2018)
sa, Kulagin, Blümlein, Moch, Petti hep-ph/1808.06871
sa, Blümlein, Moch hep-ph/1808.08404
sa, Blümlein, Moch hep-ph/1909.03533

HQHP19, Mainz, 8 Oct 2019

ABM PDF fit framework

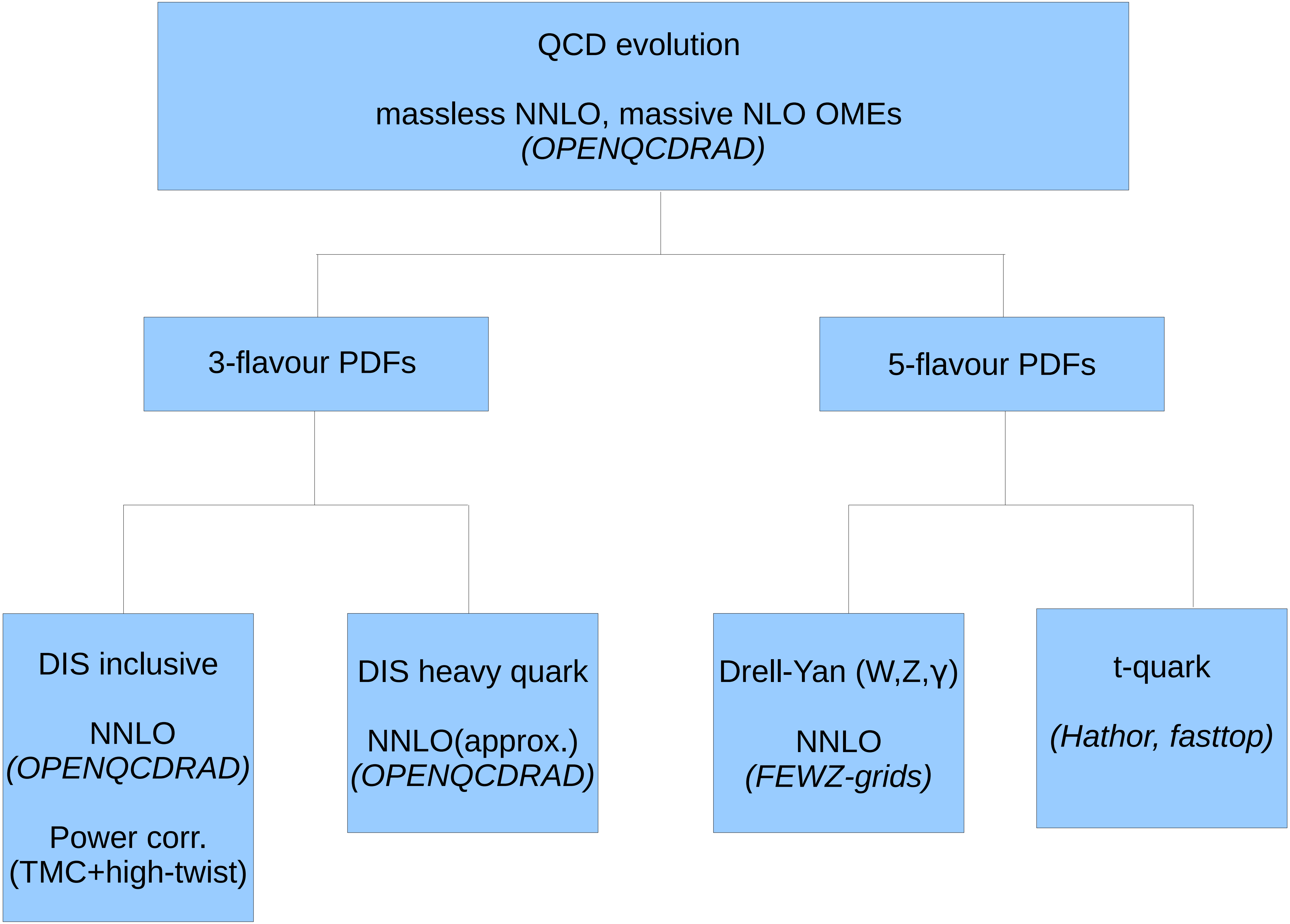

Data used and fit quality

Experiment	Process	Reference	NDP	χ^2
	DIS			
HERA I + II	$e^{\pm}p \to e^{\pm}X$	[4]	1168	1510
	$e^{\pm}p \to \overset{(-)}{\nu}X$			
BCDMS	$\mu^{+}p \to \mu^{+}X$	[61]	351	411
NMC	$\mu^{+}p \to \mu^{+}X$	[60]	245	343
SLAC-49a	$e^{-}p \to e^{-}X$	[54,62]	38	59
SLAC-49b	$e^{-}p \to e^{-}X$	[54,62]	154	171
SLAC-87	$e^{-}p \to e^{-}X$	[54,62]	109	103
SLAC-89b	$e^{-}p \to e^{-}X$	[56,62]	90	79
	DIS heavy-quark production			
HERA I + II	$e^{\pm}p \to e^{\pm}cX$	[63]	52	62
H1	$e^{\pm}p \to e^{\pm}bX$	[15]	12	5
ZEUS	$e^{\pm}p \to e^{\pm}bX$	[16]	17	16
CCFR	$\overset{(-)}{\nu}N \to \mu^{\pm}cX$	[64]	89	62
CHORUS	$\nu N \to \mu^{+}cX$	[18]	6	7.6
NOMAD	$\nu N \to \mu^{+}cX$	[17]	48	59
NuTeV	$\overset{(-)}{\nu}N \to \mu^{\pm}cX$	[64]	89	49
	DY			
FNAL-605	$pCu \to \mu^{+}\mu^{-}X$	[68]	119	165
FNAL-866	$pp \to \mu^{+}\mu^{-}X$	[69]	39	53
	$pD \to \mu^{+}\mu^{-}X$			
	Top-quark production			
ATLAS, CMS	$pp \to tqX$	[27–32]	10	2.3
CDF&DØ	$\bar{p}p \to tbX$	[53]	2	1.1
	$\bar{p}p \to tqX$			
ATLAS, CMS	$pp \to t\bar{t}X$	[33–52]	23	13
CDF&DØ	$\bar{p}p \to t\bar{t}X$	[53]	1	0.2

DY data in the ABMP16 fit

Experiment	ATLAS		CMS		DØ		LHCb		
$\sqrt{s}$ (TeV)	7	13	7	8	1.96		7	8	
Final states	$W^+ \to l^+\nu$ $W^- \to l^-\nu$ $Z \to l^+l^-$	$W^+ \to l^+\nu$ $W^- \to l^-\nu$ $Z \to l^+l^-$	$W^+ \to \mu^+\nu$ $W^- \to \mu^-\nu$ (asym)	$W^+ \to \mu^+\nu$ $W^- \to \mu^-\nu$	$W^+ \to \mu^+\nu$ $W^- \to \mu^-\nu$ (asym)	$W^+ \to e^+\nu$ $W^- \to e^-\nu$ (asym)	$W^+ \to \mu^+\nu$ $W^- \to \mu^-\nu$ $Z \to \mu^+\mu^-$	$Z \to e^+e^-$	$W^+ \to \mu^+\nu$ $W^- \to \mu^-\nu$ $Z \to \mu^+\mu^-$
Cut on the lepton P_T	$P^l_T > 20$ GeV	$P^e_T > 25$ GeV	$P^\mu_T > 25$ GeV	$P^\mu_T > 25$ GeV	$P^\mu_T > 25$ GeV	$P^e_T > 25$ GeV	$P^\mu_T > 20$ GeV	$P^e_T > 20$ GeV	$P^\mu_T > 20$ GeV
Luminosity (1/fb)	0.035	0.081	4.7	18.8	7.3	9.7	1	2	2.9
NDP	30	6	11	22	10	13	31(33) [a]	17	32(34)
ABMP16	31.0	9.2	22.4	16.5	17.6	19.0	45.1(54.4)	21.7	40.0(59.2)
CJ15	–	–	–	–	20	29	–	–	–
CT14	42	–	– [b]	–	–	34.7	–	–	–
HERAFitter	–	–	–	–	13	19	–	–	–
MMHT16	39 [c]	–	–	21	21 [c]	26	(43)	29	(59)
NNPDF3.1	29	–	19	–	16	35	(59)	19	(47)

[a] The values of NDP and χ^2 correspond to the unfiltered samples.
[b] For the statistically less significant data with the cut of $P^\mu_T > 35$ GeV the value of $\chi^2 = 12.1$ was obtained.
[c] The value obtained in MMHT14 fit.

Experiment	NDP	χ^2 after the data sets excuded				
		–	ATLAS	CMS	DØ	LHCb
ATLAS	36	37.7	–	37.0	38.3	39.6
CMS	33	26.6	25.6	–	26.0	23.5
DØ	23	48.5	48.1	47.7	–	**44.2**
LHCb	80	98.2	100.2	97.4	**78.8**	–

- Good overall agreement in NNLO with some tension between D0 and LHCb data

NNLO tools

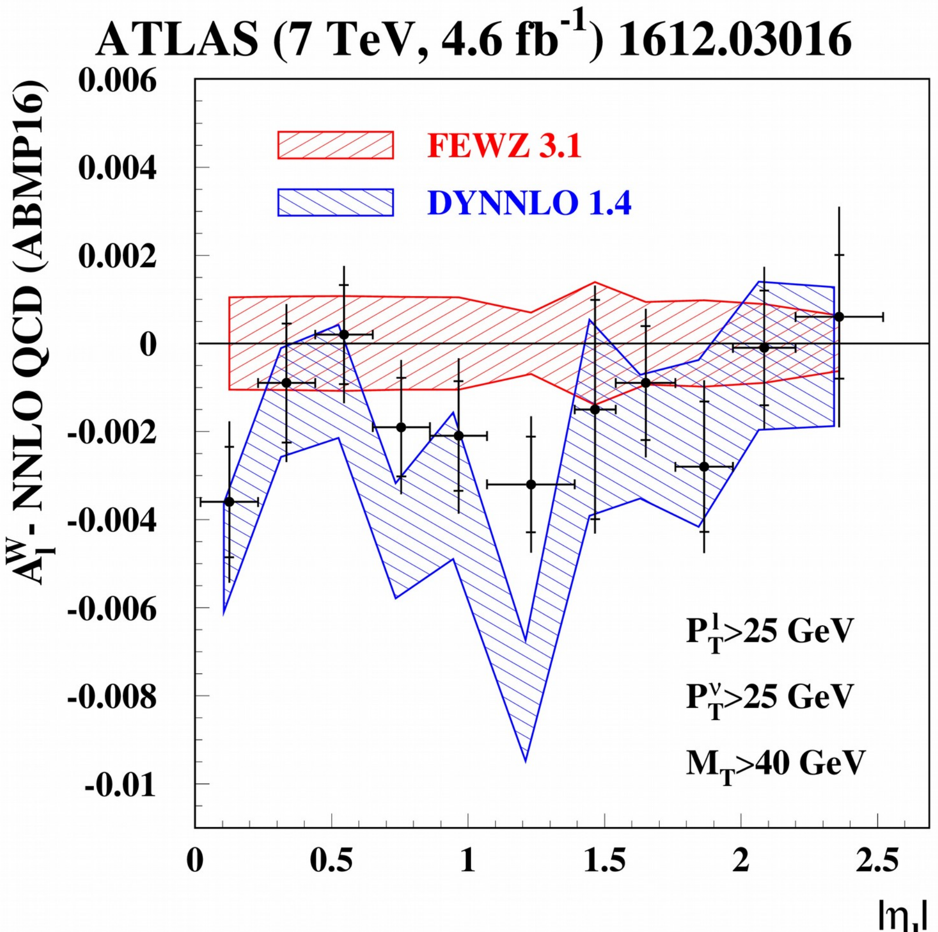

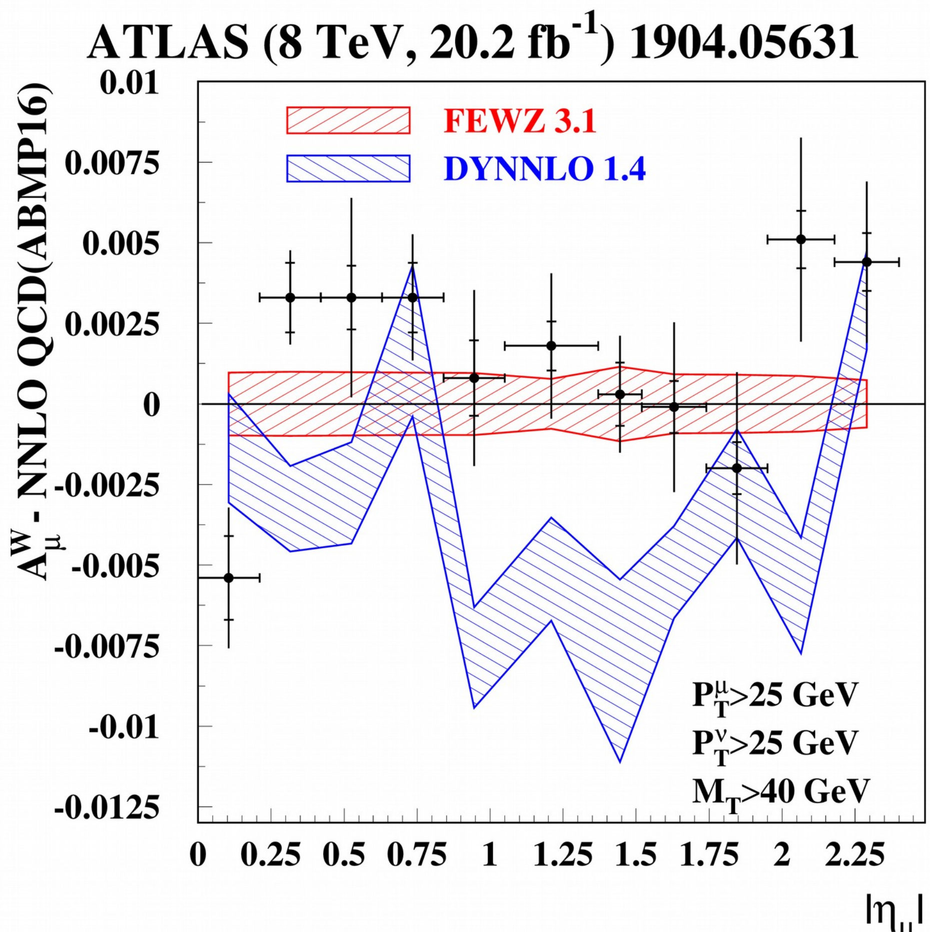

The bands display an integration accuracy obtained with O(month) of the wall time

- The FEWZ predictions somewhat overshoot the data at 7 TeV, while the DYNNLO ones go lower and are in better agreement with the measurements

- At 8 TeV the tendency is different: The FEWZ predictions somewhat undershoot the data and the DYNNLO ones go essentially lower

- FEWZ predictions demonstrate better overall agreement with the data therefore this tool is routinely used in the fit

Most recent DY inputs

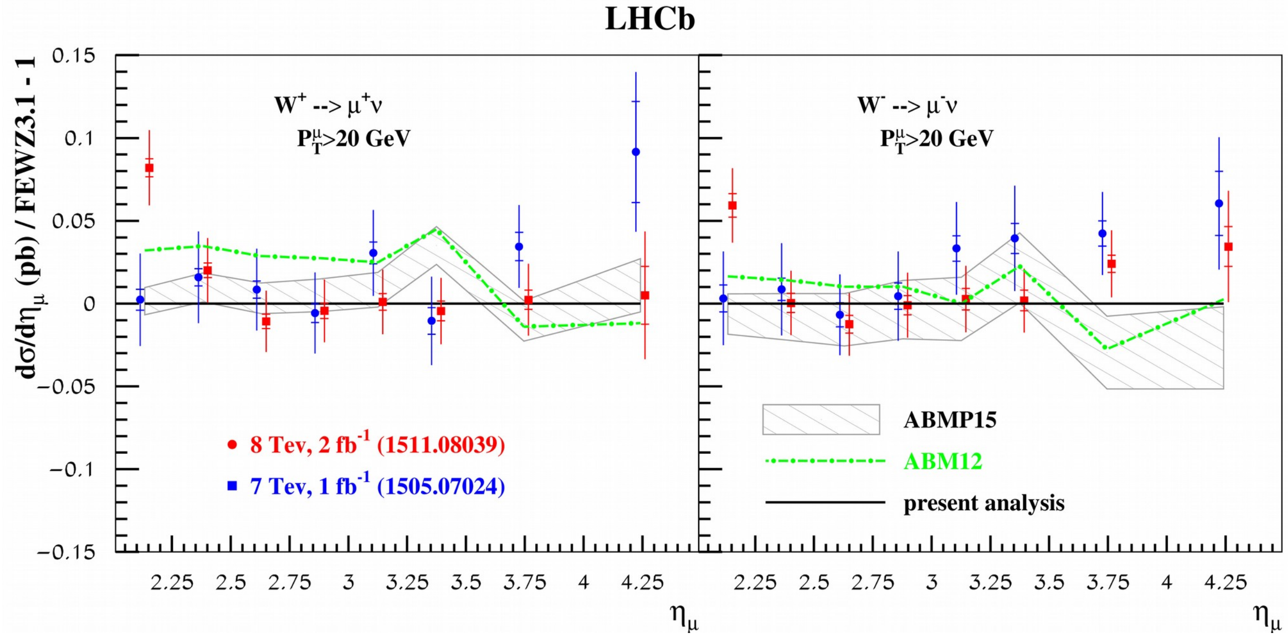

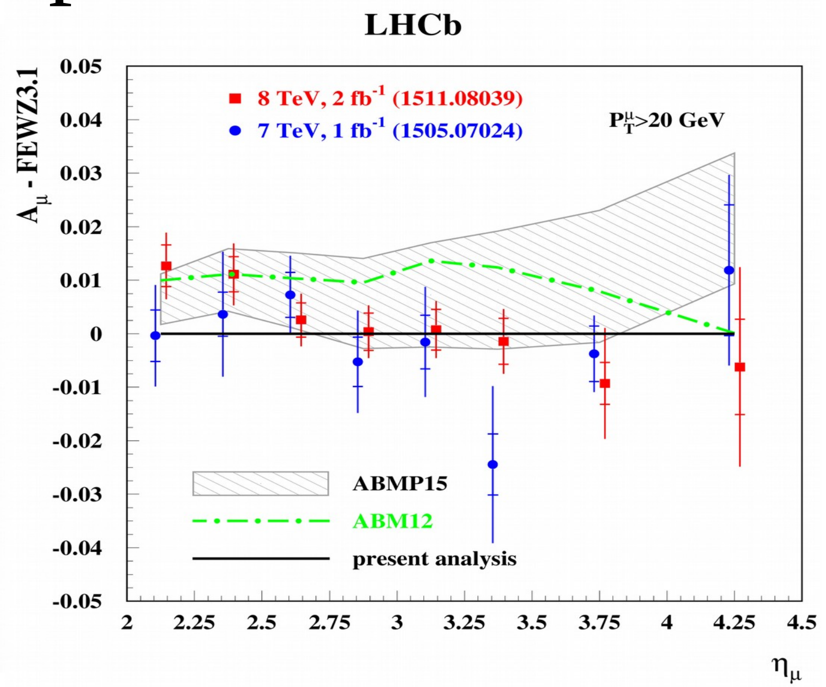

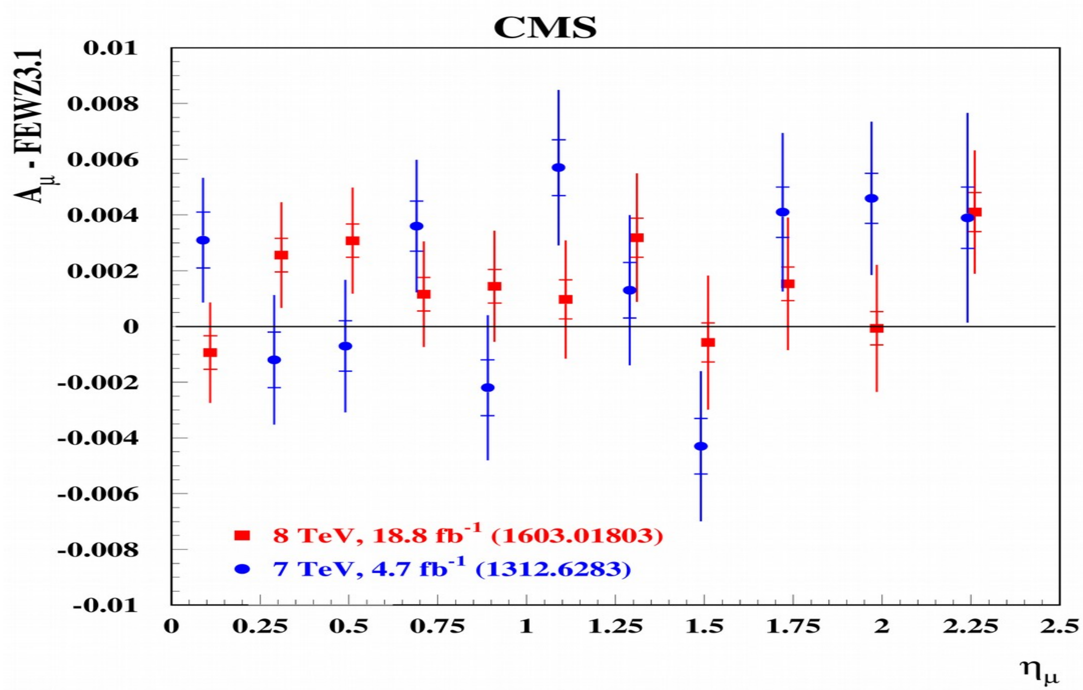

Filtering of the LHCb data has been performed:

– a bump at 7 Tev and Y=3.275
(not confirmed by the LHCb data at 8 TeV)

– and excess at 8 TeV and Y=2.125
(not confirmed by the CMS data at 8 TeV)

The CMS data at 8 TeV are much smoother than the ones at 7 TeV:

χ^2=17/22 versus 22/11

Impact of the W-, Z-data

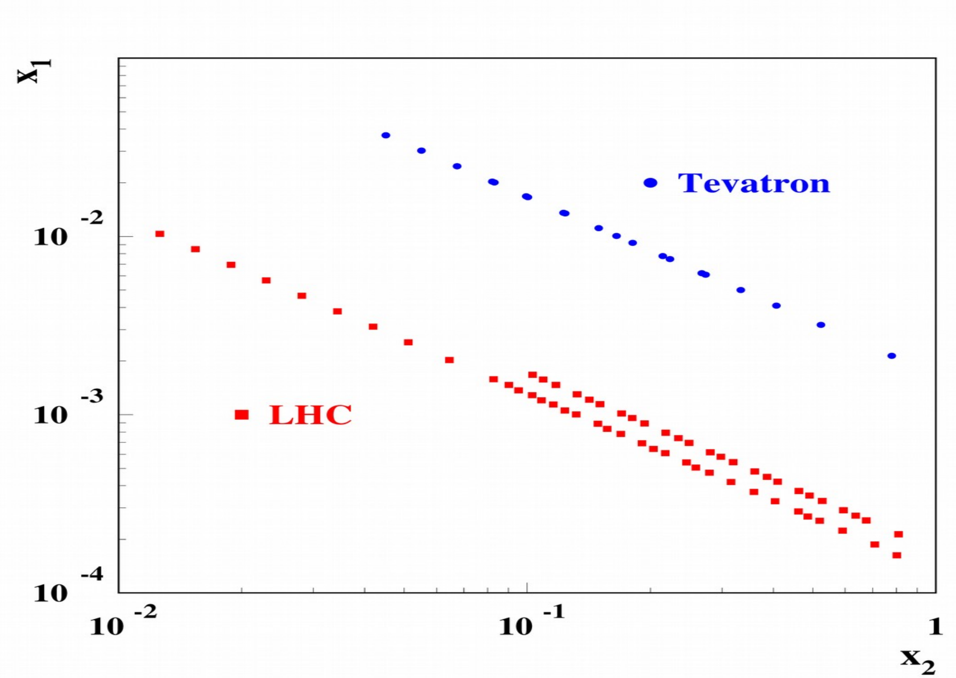

In the forward region $x_2 >> x_1$

$\sigma(W^+) \sim u(x_2)\ \text{dbar}\ (x_1)$

$\sigma(W^-) \sim d(x_2)\ \text{ubar}(x_1)$

$\sigma(Z) \sim Q_U^2 u(x_2)\ \text{ubar}\ (x_1) + Q_D^2 d(x_2)\ \text{dbar}(x_1)$

$\sigma(DIS) \sim q_u^2 u(x_2) + q_d^2 d(x_2)$

Forward W&Z production probes small/large x and is complementary to the DIS ⇒ good quark disentangling

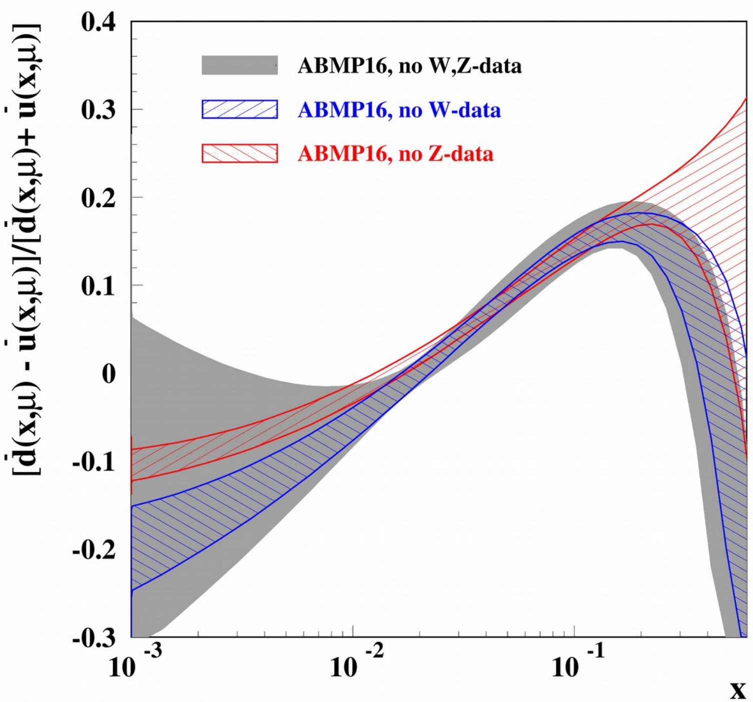

Negative small-x sea isospin asymmetry

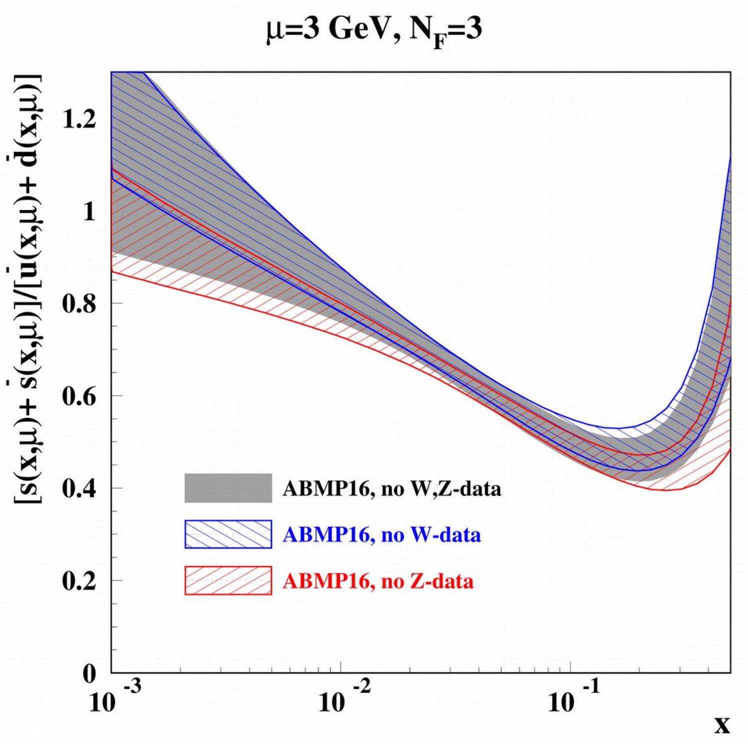

No small-x strange sea suppression at small x

d/u at large x

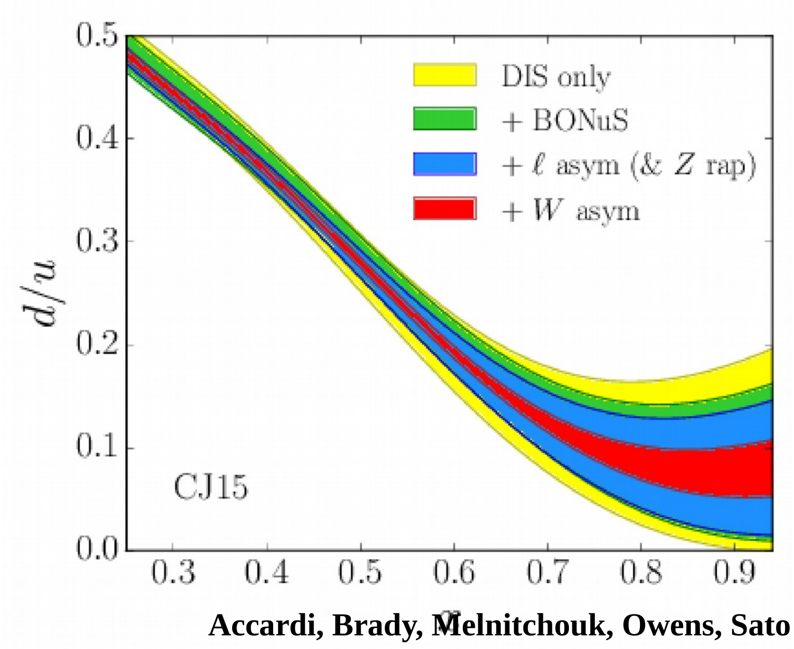

Accardi, Brady, Melnitchouk, Owens, Sato PRD 93, 114017 (2016)

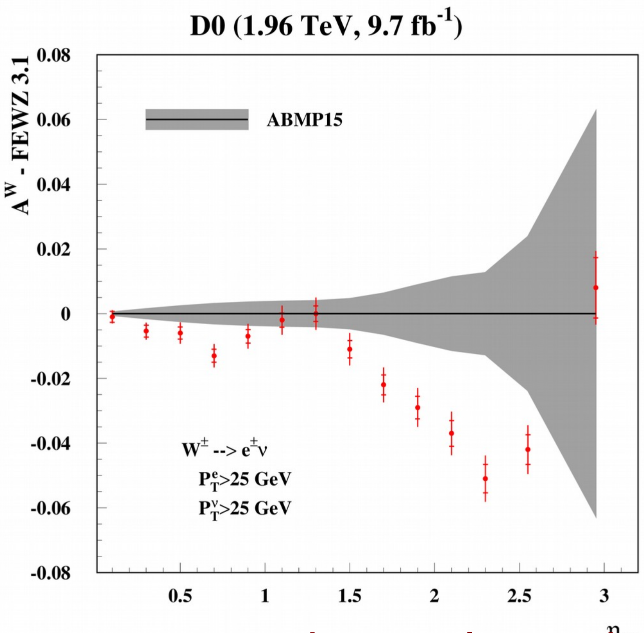

W-asymmetry data go lower that predictions based on the e-asymmetry: data selection is important

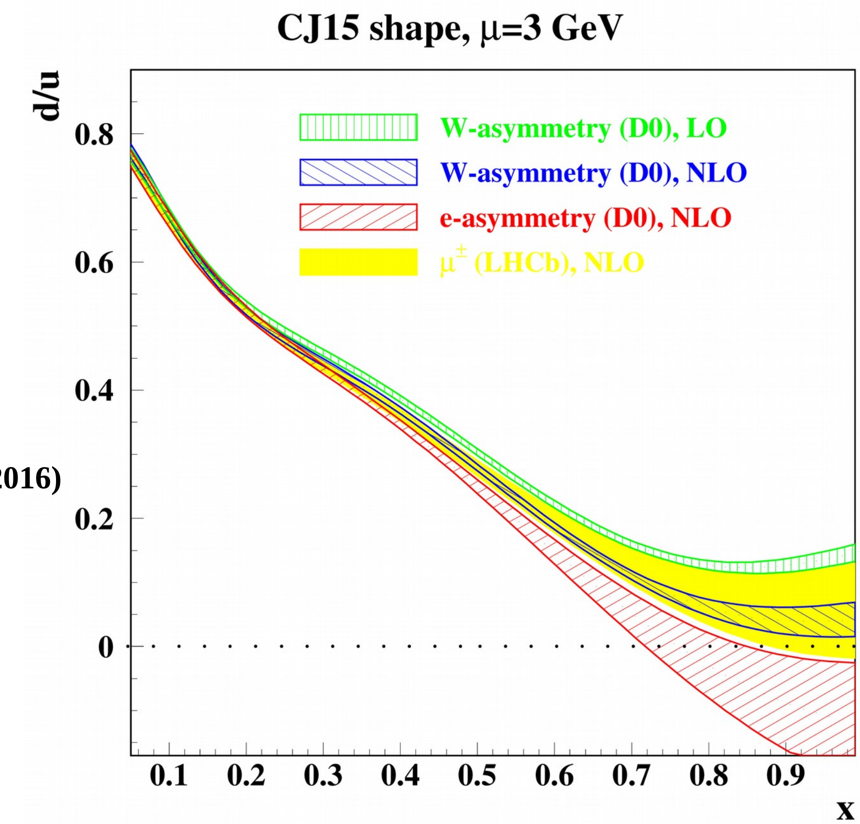

- Account of the NNLO corrections moves large-x d/u downwards
- e-asymmetry data prefer lower d/u
- d/u consistent with 0 at x → 1

Recent W and Z 7-TeV ATLAS data

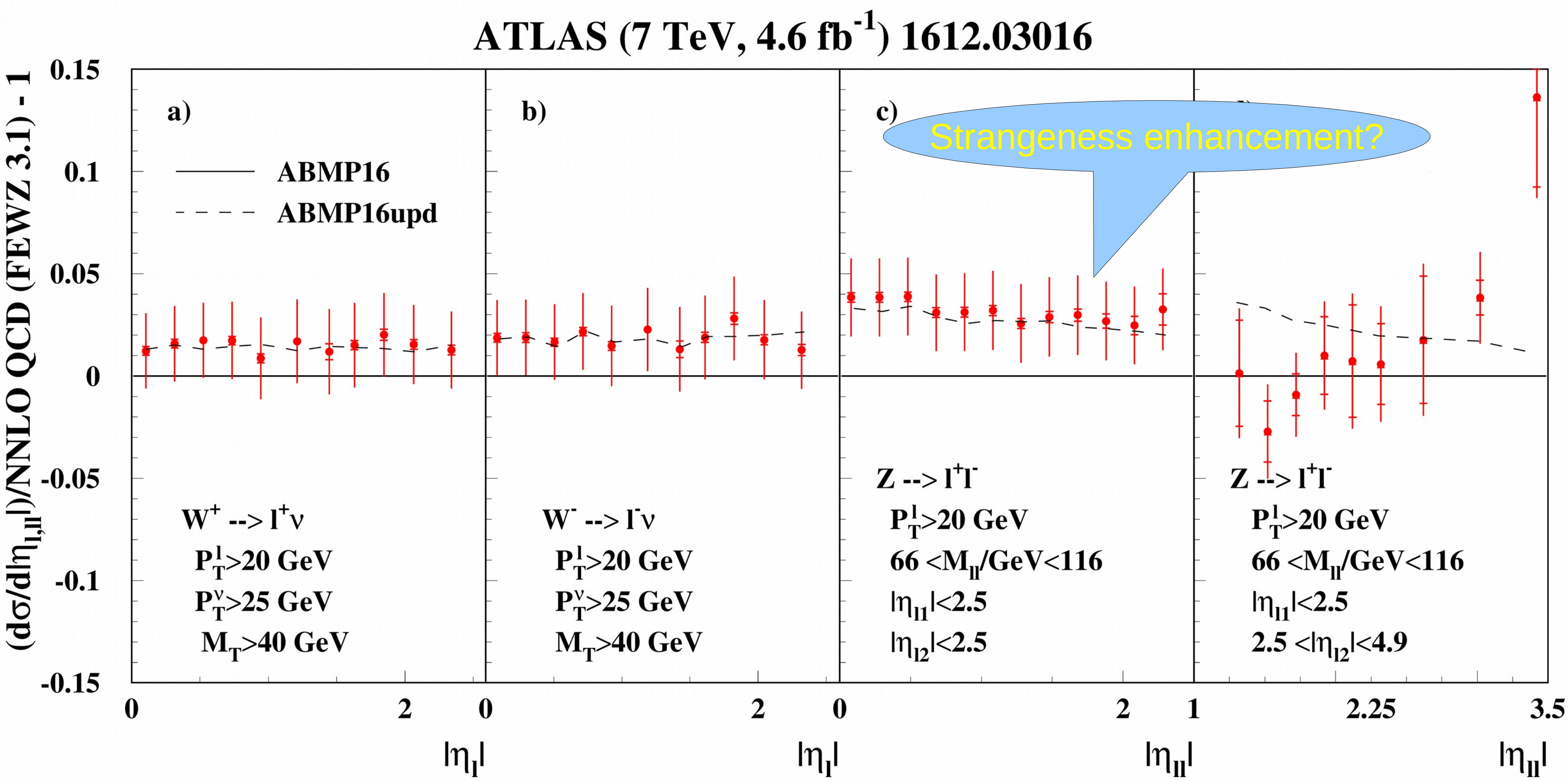

Data are well accommodated in general; forward Z-boson data have particular trend, however, χ^2 is also not bad due to large errors, 68/61 for the whole sample

Impact of ATLAS data on strangeness

	$\kappa_s(\mu^2=20\ \mathrm{GeV}^2)$
HERA+ATLAS	0.81(18)
HERA+ATLAS+E866	0.72(8)
ABMP16(incl. NOMAD)	0.66(3)

κ_s is integral strange sea suppression factor:

$$\kappa_s(\mu^2) = \frac{\int_0^1 x[s(x,\mu^2)+\bar{s}(x,\mu^2)]dx}{\int_0^1 x[\bar{u}(x,\mu^2)+\bar{d}(x,\mu^2)]dx},$$

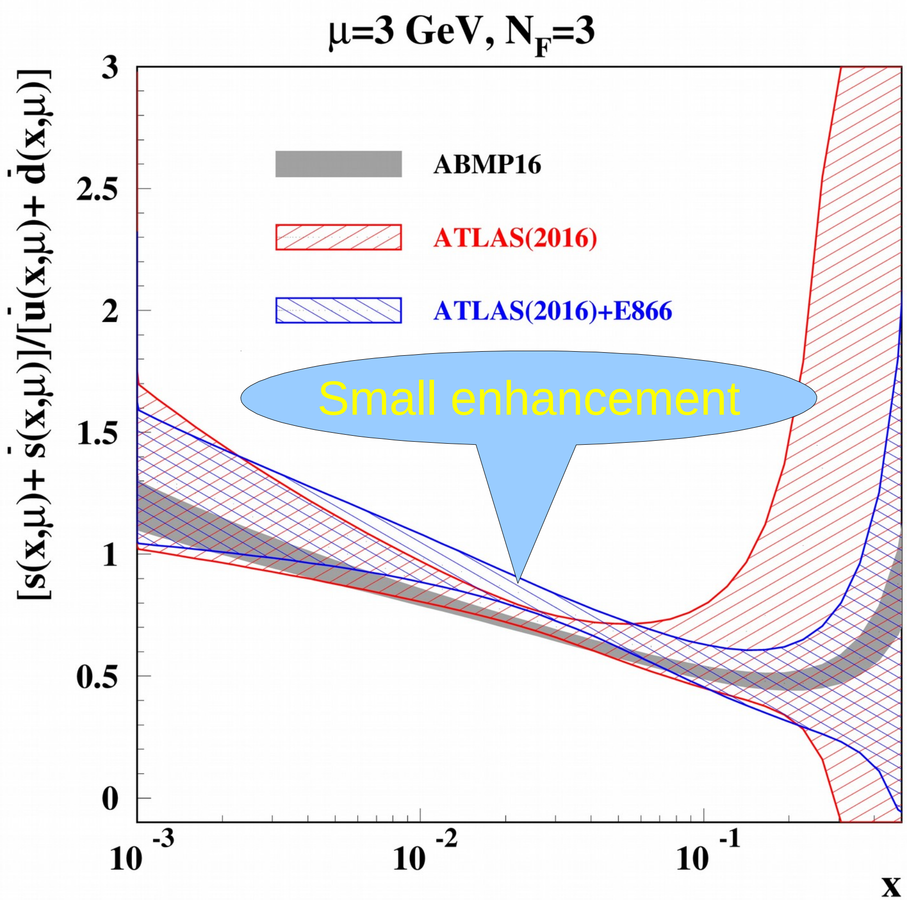

sa, Blümlein, Moch PLB 777, 134 (2018)

- ATLAS data provide a constraint on small-x sea quarks; at at moderate x additional constraint is needed, comes form fixed-target DY (FNAL-E866)
- The E866 data are consistent with the ATLAS(2016) central data: χ^2/NDP=48/39 and 40/34, respectively
- The strangeness is in a broad agreement with the one extracted from the dimuon data

Non-resonant DY 7-TeV ATLAS data

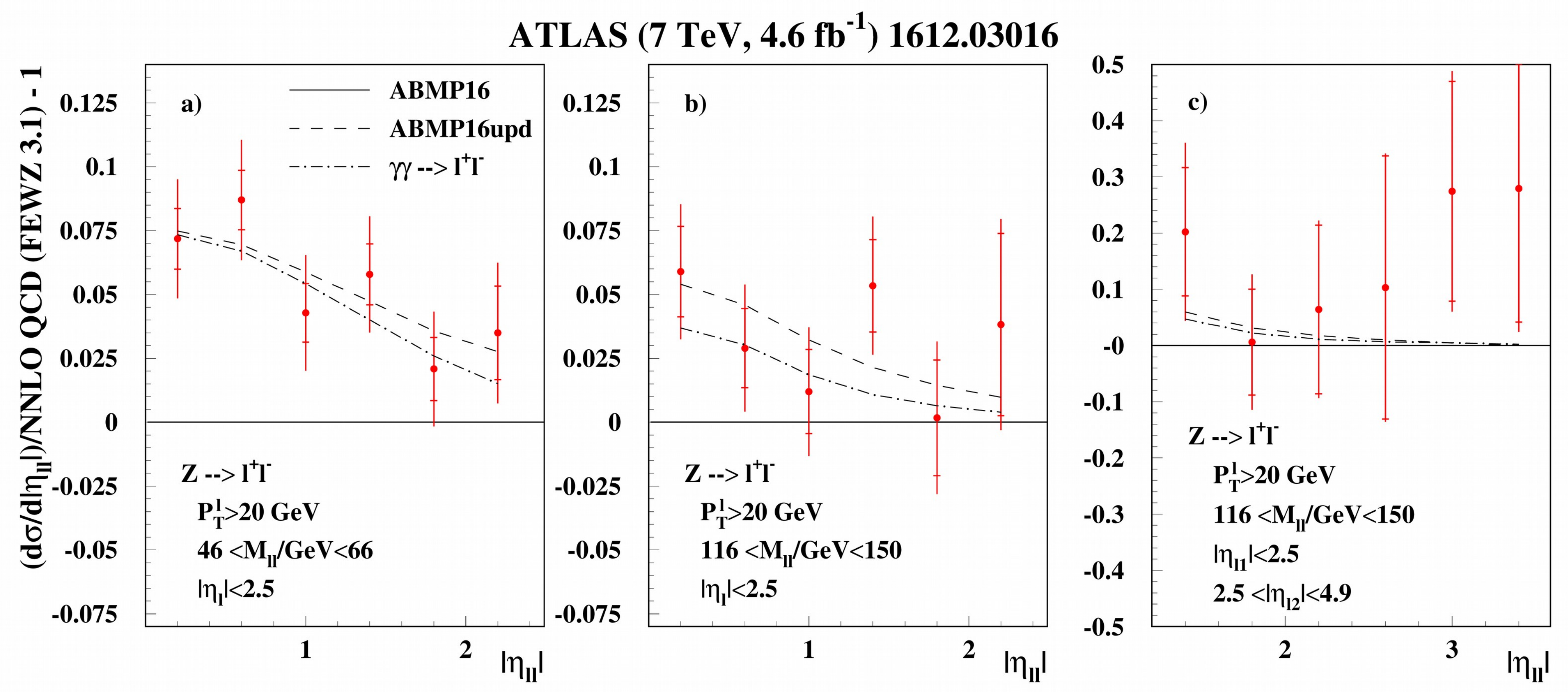

- Complementary constraint on PDFs → improved quark disentangling

$$\sigma_{DY} \sim q_u^2 u(x_2)\ \mathrm{ubar}\ (x_1) + q_d^2 d(x_2)\ \mathrm{dbar}(x_1)$$

$$\sigma_{DIS} \sim q_u^2 u(x_2) + q_d^2 d(x_2)$$

- Additional photon-photon contribution (in LO) improves agreement → photon distribution can be extracted from the data

Comined Run I+II HERA data

H1 and ZEUS EPJC 75, 580 (2015)

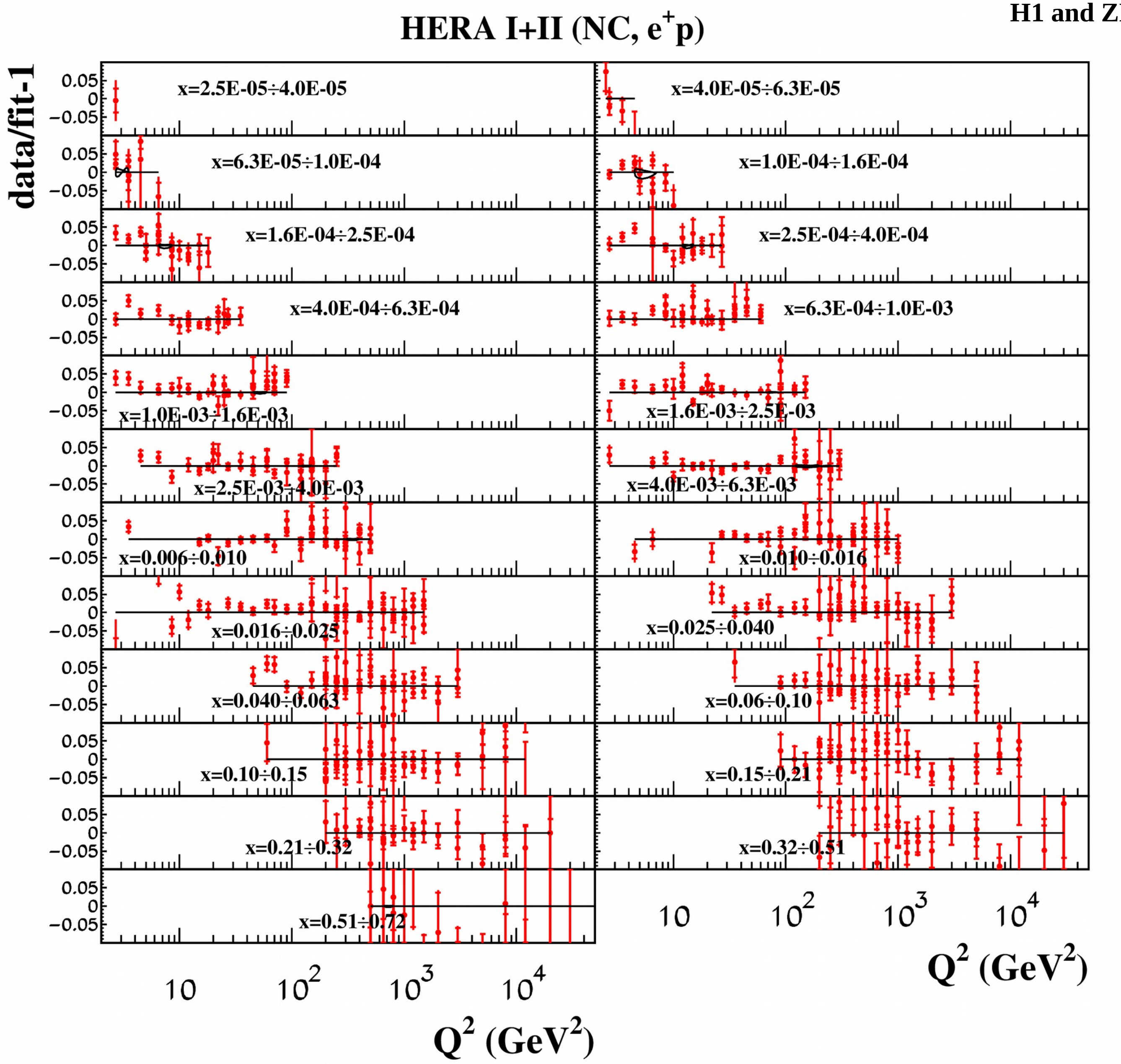

Contribution of c-quarks up to 30% at small x ⇒ *accurate treatment is required*

FFN and VFN schemes

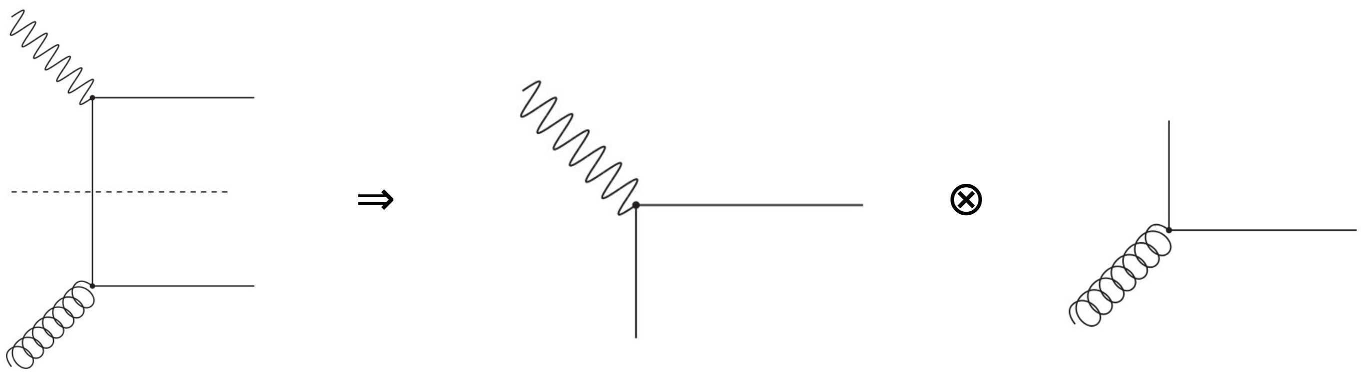

Collins, Tung NPB 278, 934 (1986)

$$H_{g,2}^{\mathrm{asymp}} = a_s(N_f) A_{hg}^{(1)}$$

Asymptotic 3-flavor coefficient function

LO:

$$A_{ij}^{(1)}\left(z, \frac{m_h^2}{\mu^2}\right) = a_{ij}^{(1,1)}(z) \ln\left(\frac{\mu^2}{m_h^2}\right)$$

Massive operator matrix elements (OMEs)

$$h^{(1)}(x,\mu^2) = a_s(N_f+1,\mu^2)\left[A_{hg}^{(1)}\left(\frac{m_h^2}{\mu^2}\right) \otimes G^{(2)}\left(N_f,\mu^2\right)\right](x)$$

Matching condition for the heavy-quark PDFs

$$F_{g,2}^{\mathrm{asymp}} = e_h^2 x h^{(1)}(x,\mu^2)$$

NLO: $\cdots$

Buza, Matiounine, Smith, van Neerven EPJC 1, 301 (1998)

$$A_{ij}^{(2)}\left(z, \frac{m_h^2}{\mu^2}\right) = a_{ij}^{(2,2)}(z) \ln^2\left(\frac{\mu^2}{m_h^2}\right) + a_{ij}^{(2,1)}(z) \ln\left(\frac{\mu^2}{m_h^2}\right) + a_{ij}^{(2,0)}(z)$$

2-mass contributions in NLO and NNLO

Blümlein et al. PLB 782, 362 (2018)

NNLO: log-terms; constant terms up to the gluonic one

Blümlein, et al., work in progress

- The VFN scheme works well at $\mu \gg m_h$ (W,Z,t-quark production,....)
- Problematic for DIS ⇒ additional modeling of power-like terms required at small scales (ACOT, BMSN, FONLL, RT....)

Heavy-quark electro-production with FFN

- Only 3 light flavors appear in the initial state
- The dominant mechanism is photon-gluon fusion
- The coefficient functions up to the NLO

  Witten NPB 104, 445 (1976)

  Laenen, Riemersma, Smith, van Neerven NPB 392, 162 (1993)

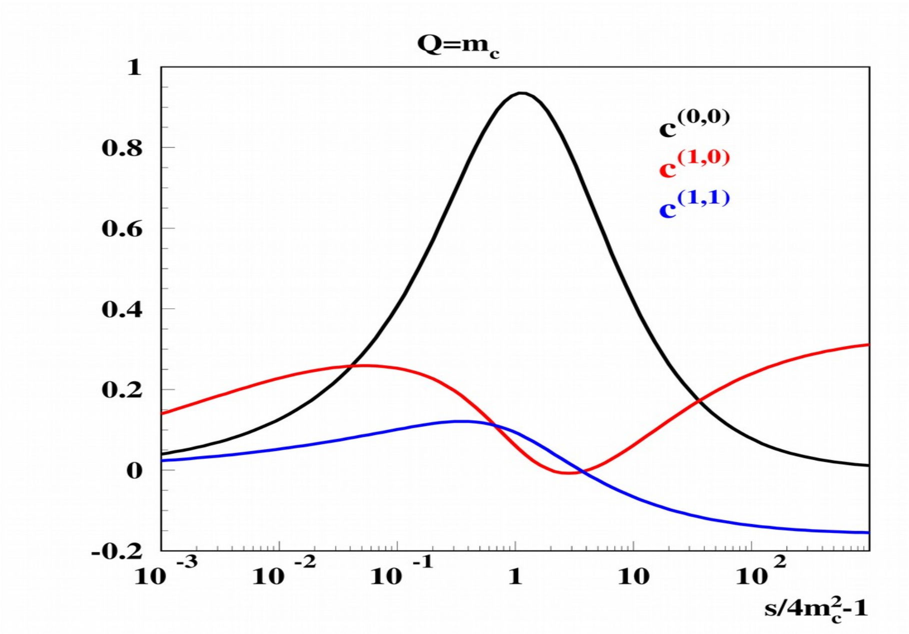

- Involved high-order calculations:
  - NNLO terms due to threshold resummation

    Laenen, Moch PRD 59, 034027 (1999)
    Lo Presti, Kawamura, Lo Presti, Moch, Vogt NPB 864, 399 (2012)

  - NNLO Mellin moments

    Ablinger at al. NPB 844, 26 (2011)

    Bierenbaum, Blümlein, Klein NPB 829, 417 (2009)

    Ablinger et al. NPB 890, 48 (2014)

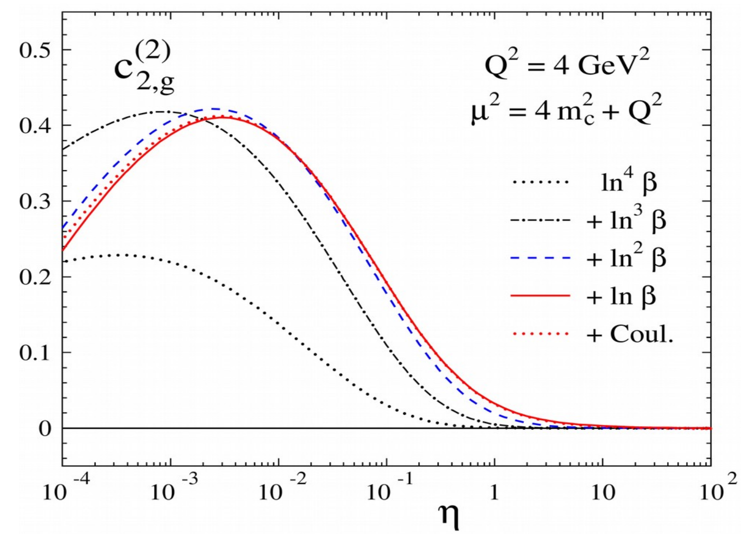

Modeling NNLO massive coefficients

small s

small x

Catani-Hautmann

s

$\xi = Q^2/m^2$

$\eta = s/4m^2 - 1$

large Q^2

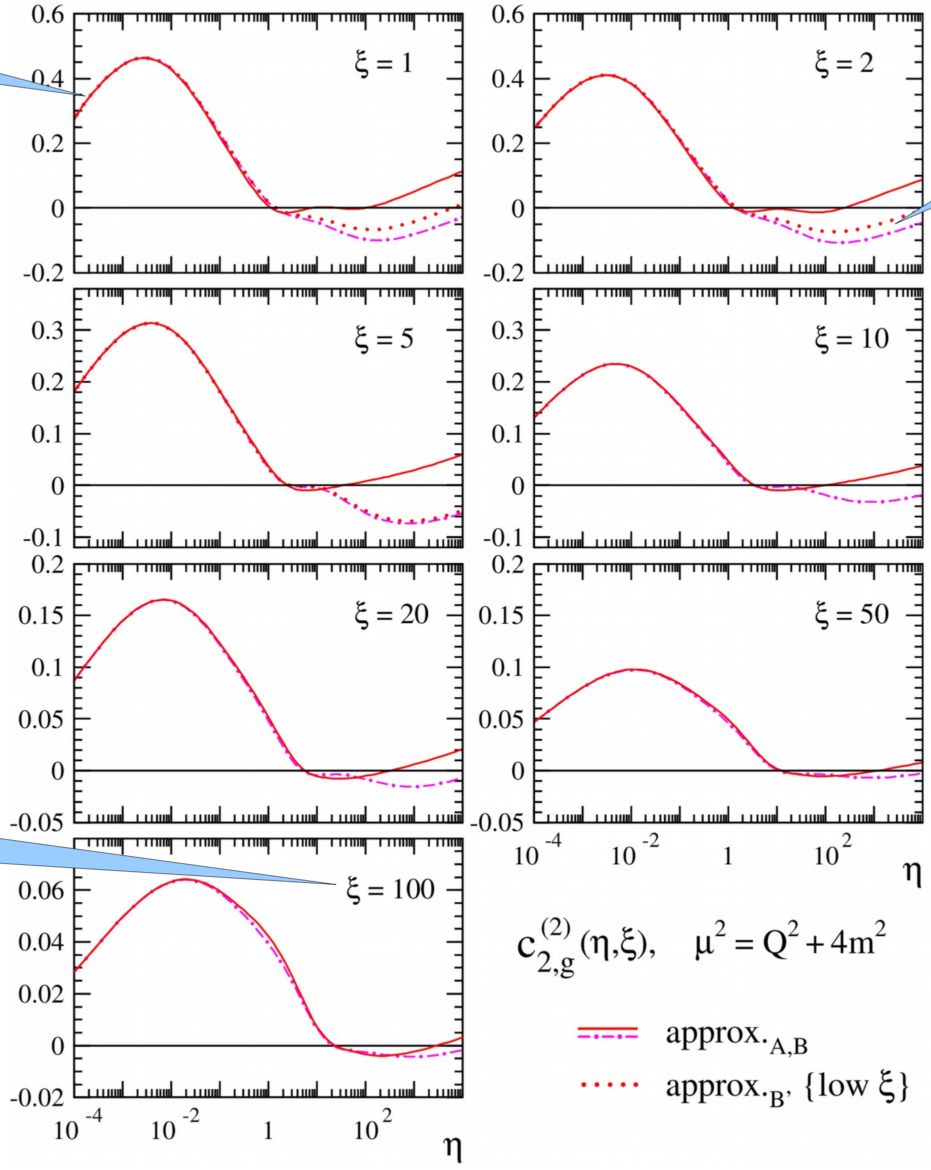

Combination of the threshold corrections (small s), high-energy limit (small x), and the NNLO massive OMEs (large Q^2) **Kawamura, Lo Presti, Moch, Vogt NPB 864, 399 (2012)**

Recent progress in FFN scheme Wilson coefficients

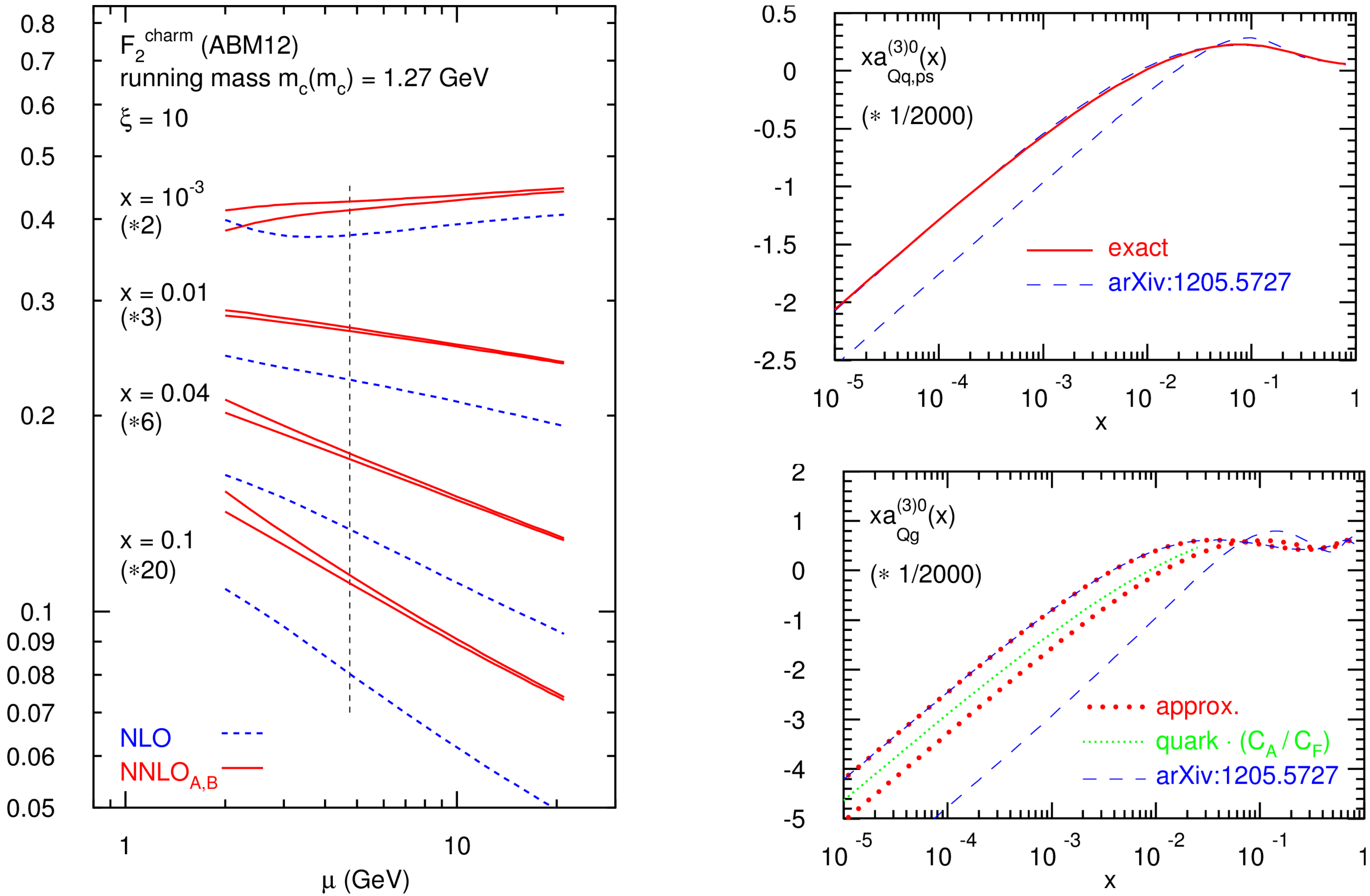

Update with the pure singlet massive OMEs → improved theoretical uncertainties

sa, Moch, Blümlein PRD 96, 014011 (2017)

Running mass in DIS

The pole mass is defined for the free (*unobserved*) quarks as a the QCD Lagrangian parameter and is commonly used in the QCD calculations

$$\mathcal{L} = -\frac{1}{4} F_{\mu\nu} F^{\mu\nu} + \sum_{\text{flavors}} \bar{q}\,(\mathrm{i}\not{D} - m_q)\, q$$

$$\not{p} - m_q - \Sigma(p, m_q)\Big|_{p^2 = m_q^2}$$

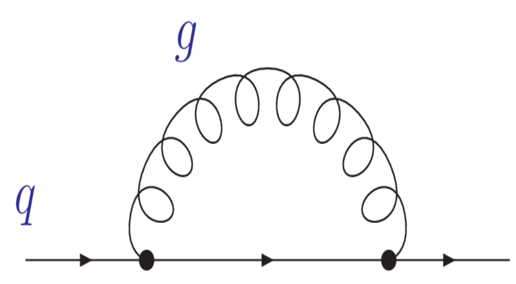

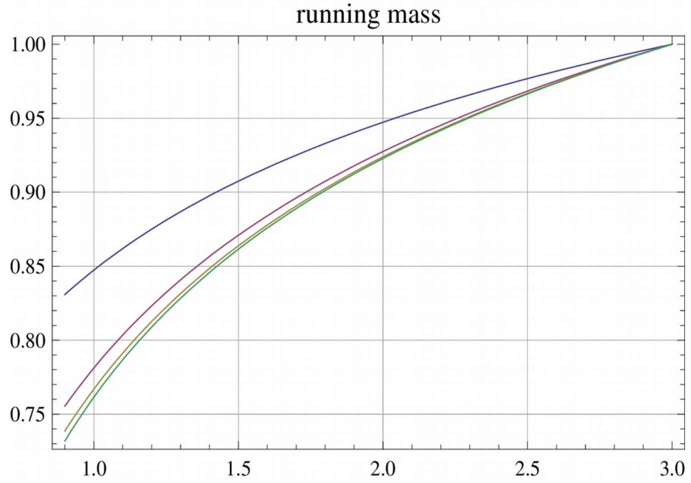

The quantum corrections due to the self-energy loop Integrals receive contribution down to scale of $O(\Lambda_{QCD})$

→ sensitivity to the high order corrections, particularly at the production threshold

$$\mu^2 \frac{d}{d\mu^2} m(\mu) = \gamma(\alpha_s) m(\mu)$$

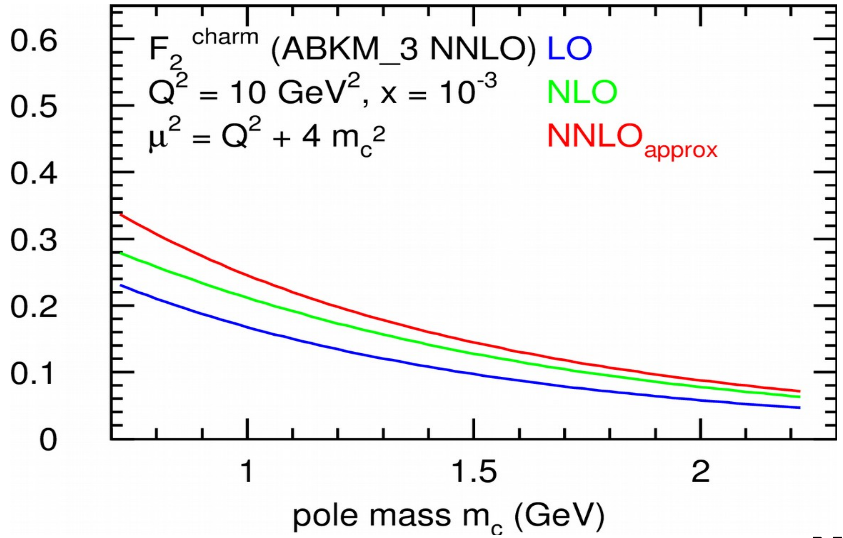

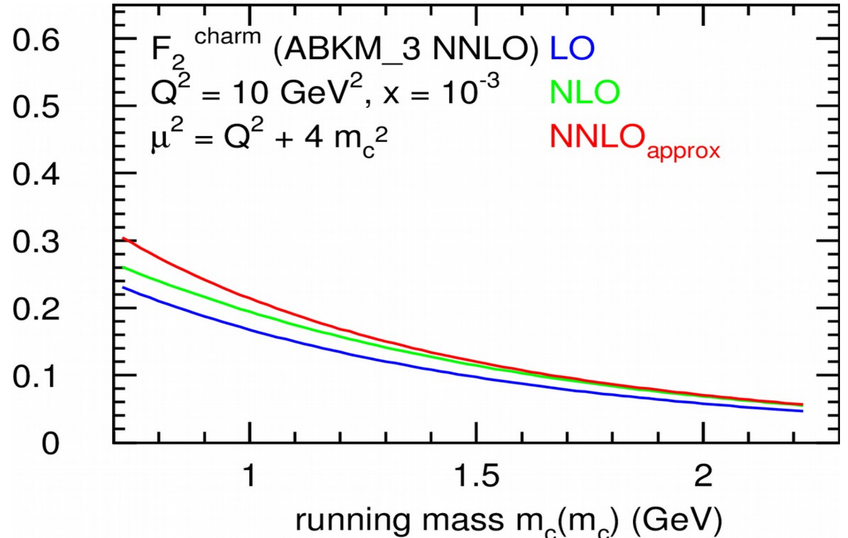

sa, Moch PLB 699, 345 (2011)

HERA charm data and m_c

H1, ZEUS EPJC 78, 473 (2018)

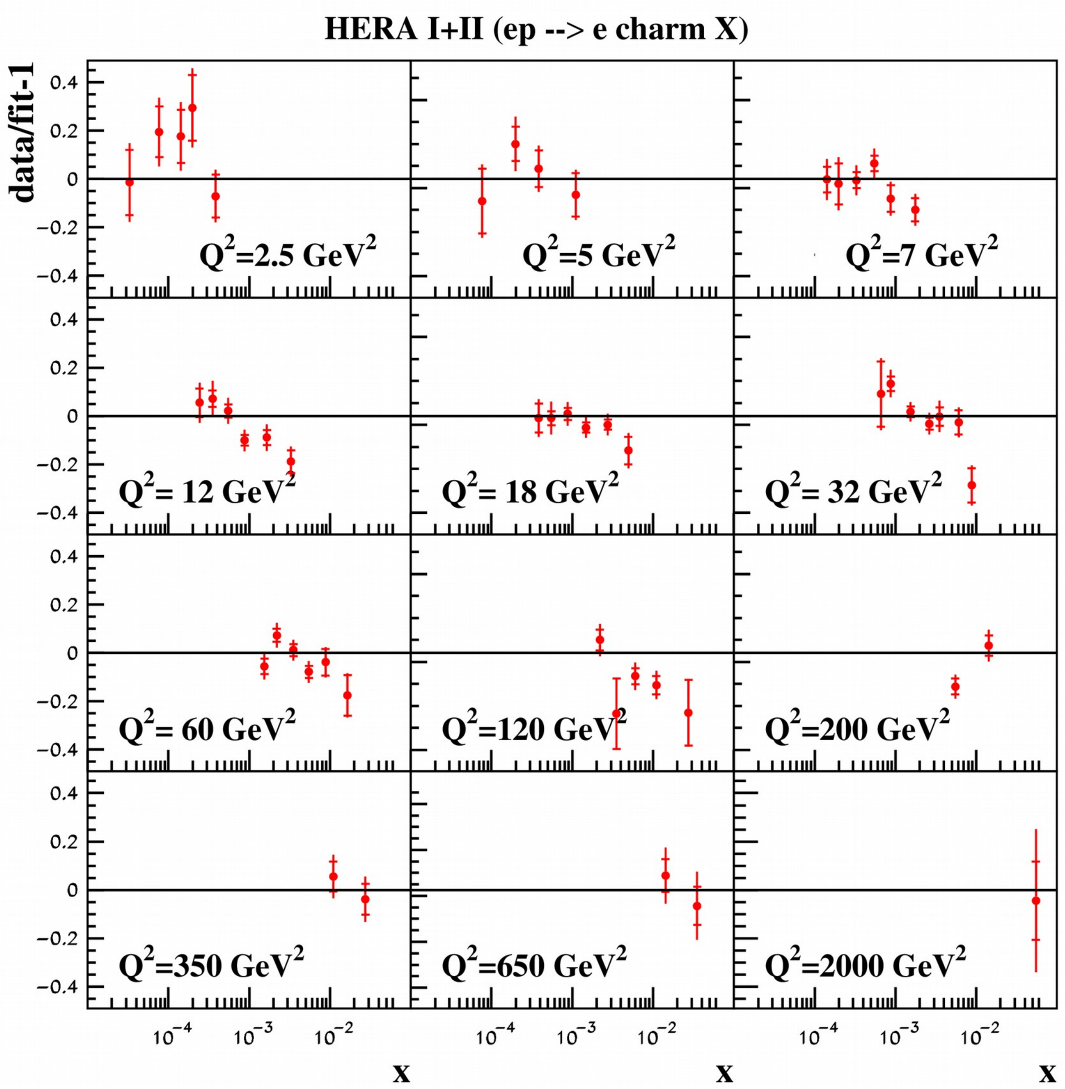

Theory: FFN scheme, running mass definition

$m_c(m_c)$=1.250±0.019(exp.) GeV

ABMP16upd

$m_c(m_c)$=1.246±0.023 (h.o.) GeV NNLO

Kiyo, Mishima, Sumino PLB 752, 122 (2016)

$m_c(m_c)$=1.279±0.008 GeV

Kühn, LoopsLegs2018

Good consistency with the earlier results and other determinations → further confirmation of the FFN scheme relevance for the HERA kinematics

Higher twists in DIS: generalities

Operator product expansion:

$F_{2,T}=F_{2,T}(\text{leading twist}) + H_{2,T}(x)/Q^2 + \ldots$ – additive

- The only one in accordance with QCD

$F_{2,T}=F_{2,T}(\text{leading twist})\,(1 + h_{2,T}(x)/Q^2 + \ldots)$ – multiplicative

- For multiplicative form the LT anomalous dimensions strongly affect the HT terms at small x

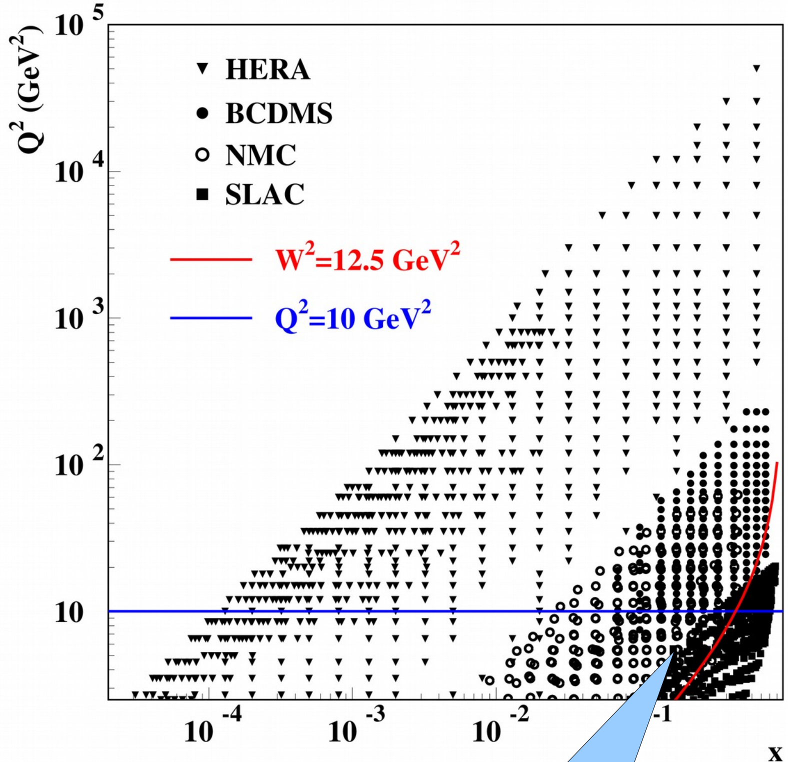

High twists appear in the DIS data at large x(equiv. W) and/or small Q2

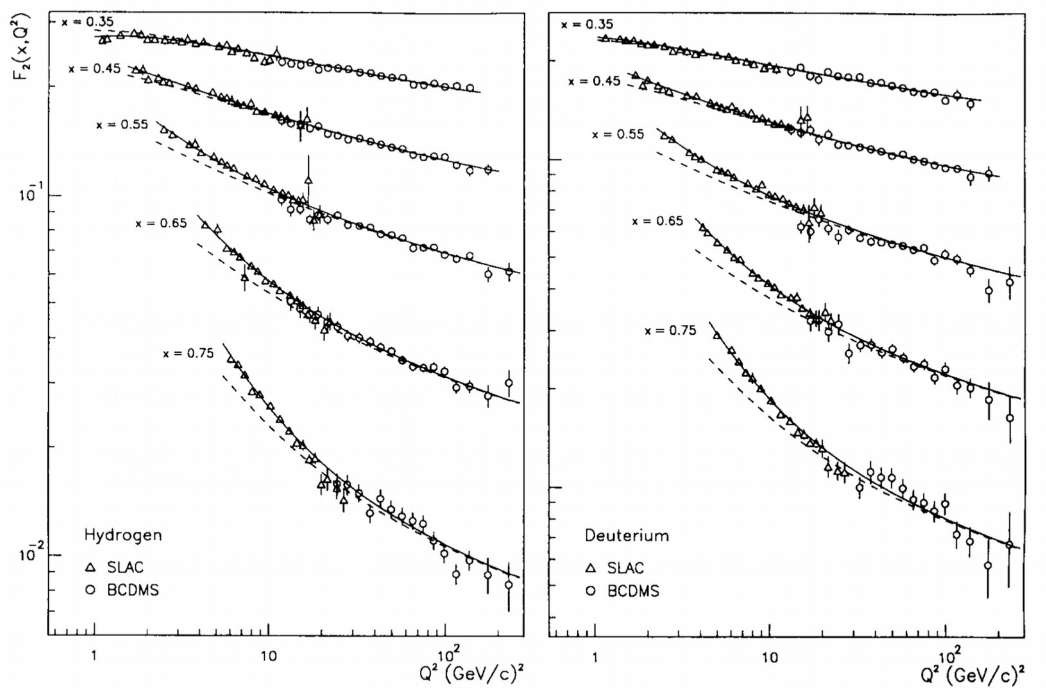

Virchaux, Milsztajn PLB 274, 221 (1992)

High twists at small x

$F_{2,T}=F_{2,T}(\text{leading twist}) + H_{2,T}(x)/Q^2$ $\qquad$ $H(x)=x^hP(x)$

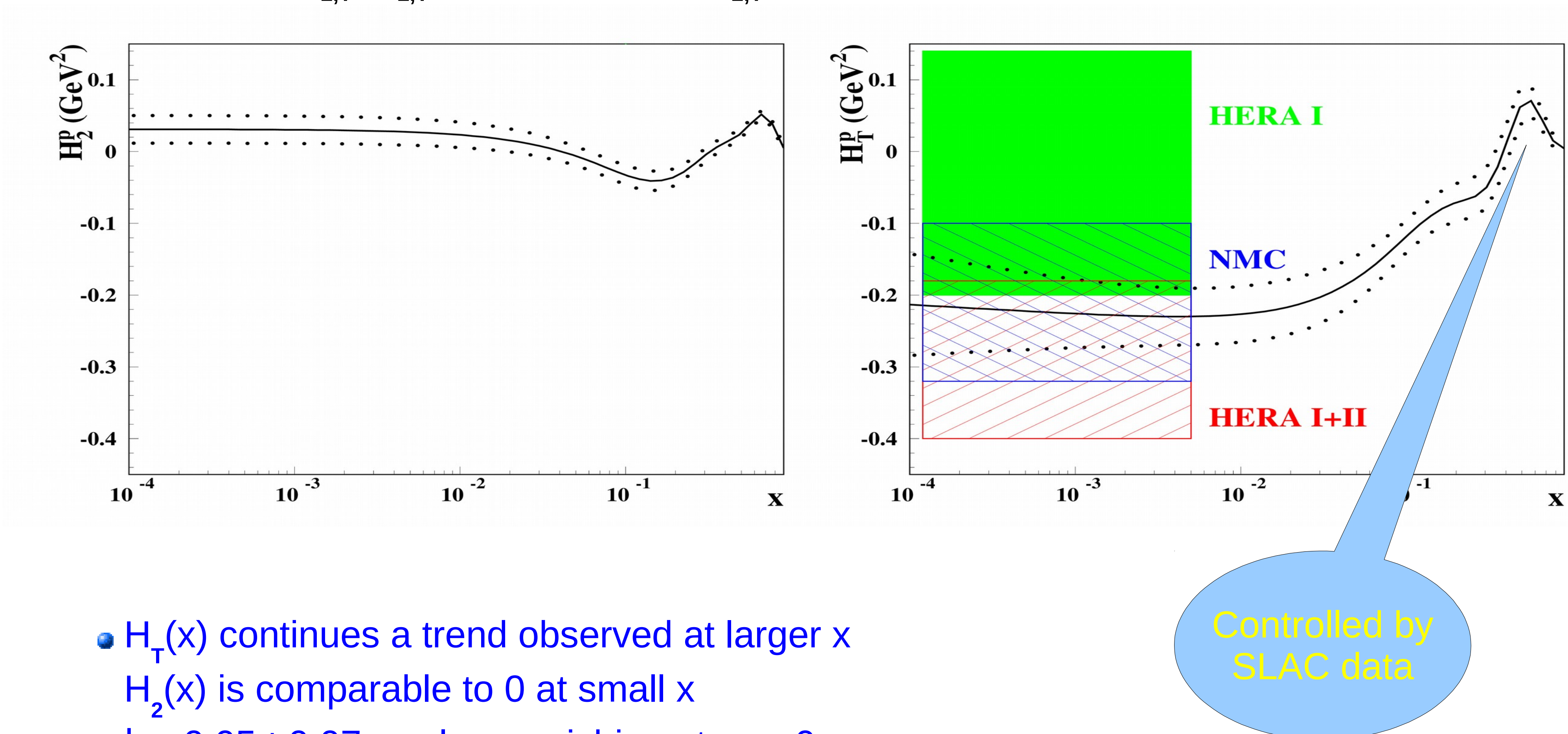

- $H_T(x)$ continues a trend observed at larger x
  $H_2(x)$ is comparable to 0 at small x
- $h_T=0.05\pm0.07$ → slow vanishing at x → 0
- Alternative explanations are considered: resummation, saturation, data defects, etc.

Correlation of α_s with twist-4 terms

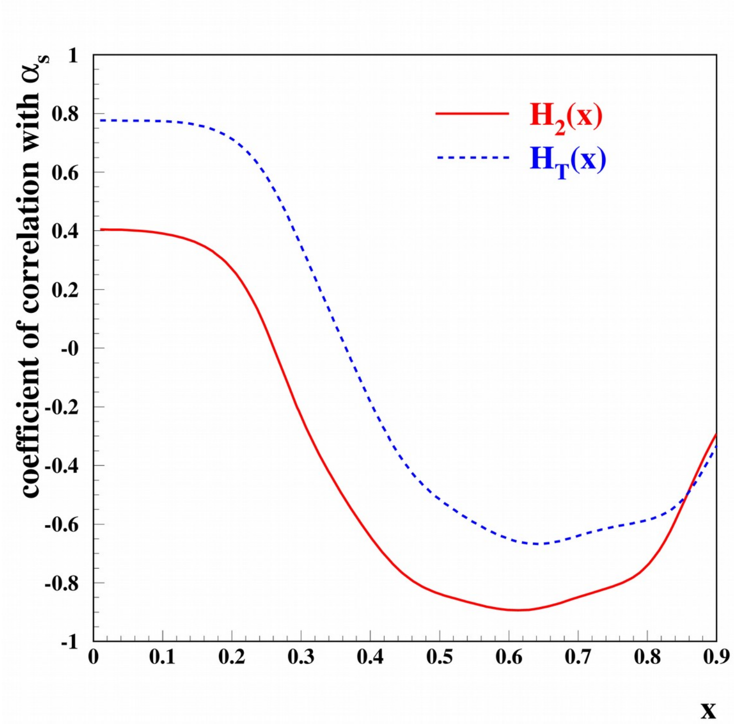

- The value of α_s and twist-4 terms are strongly correlated both at large and at small x
- With HT=0 the errors are reduced → no uncertainty due to HTs
- With account of the HT terms the value of α_s is stable with respect to the cuts

MRST: $\alpha_s(M_z)$=0.1153(20) (NNLO)
(W^2>15 GeV^2, Q^2> 10 GeV^2)

fit ansatz		$\alpha_s(M_Z)$	
higher twist modeling	cuts on DIS data	NLO	NNLO
higher twist fitted	$Q^2 > 2.5$ GeV^2, $W > 1.8$ GeV	0.1191(11)	0.1147(8)
higher twist fixed at 0	$Q^2 > 10$ GeV^2, $W^2 > 12.5$ GeV^2	0.1212(9)	0.1153(8)
	$Q^2 > 15$ GeV^2, $W^2 > 12.5$ GeV^2	0.1201(11)	0.1141(10)
	$Q^2 > 25$ GeV^2, $W^2 > 12.5$ GeV^2	0.1208(13)	0.1138(11)

A stringent cut on Q is necessary for the fit with HT=0

Small-x PDF with stringent cut on Q,W

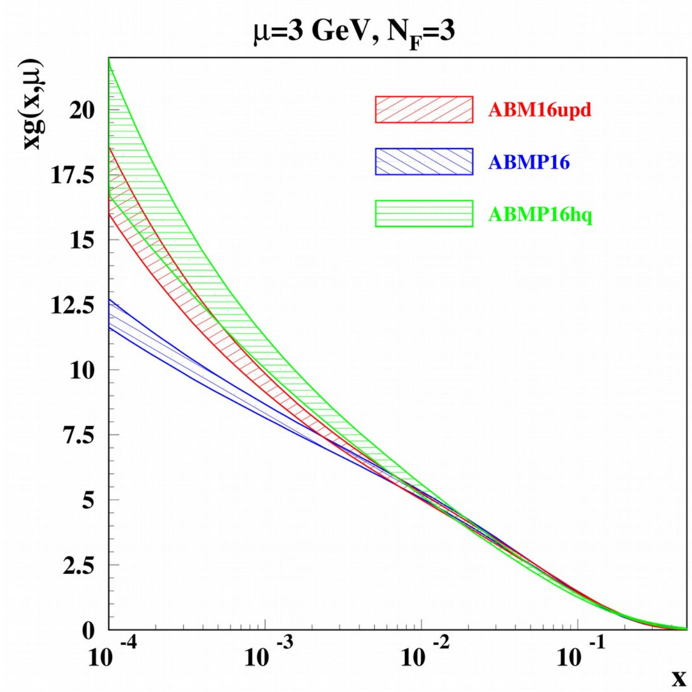

- Gluon goes higher due to more stringent cut on Q^2 (impact of the power corrections, resummations, etc. is reduced)
- Updated charm/beauty data are consistent with such an enhancement

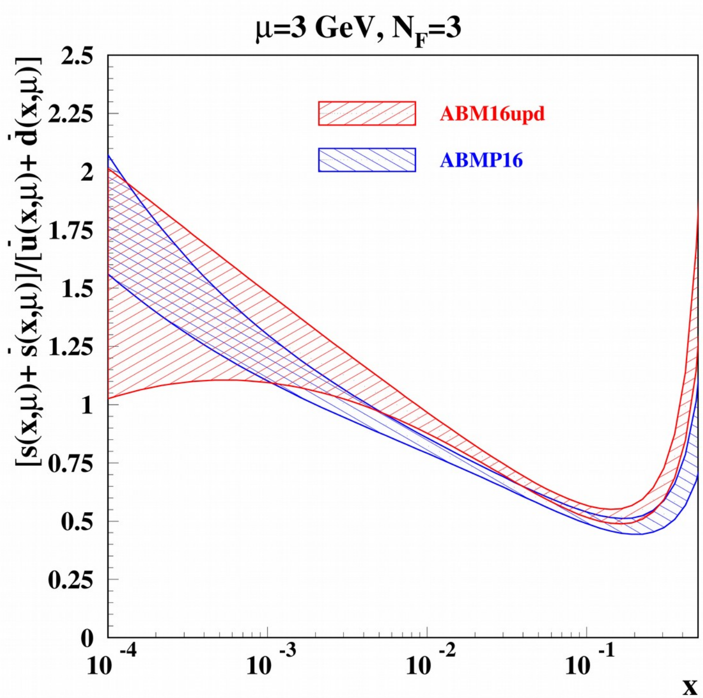

- Strange sea suppressoin factor goes lower at small x, consistent with 1 within errors
- At moderate x the strange sea is still suppressed, although integral suppression factor $\kappa_s(20\ \mathrm{GeV}^2)$=0.71(3), a little larger than 0.66(3) for ABMP16 fit due to recent ATLAS data included

Impact of t-quark data

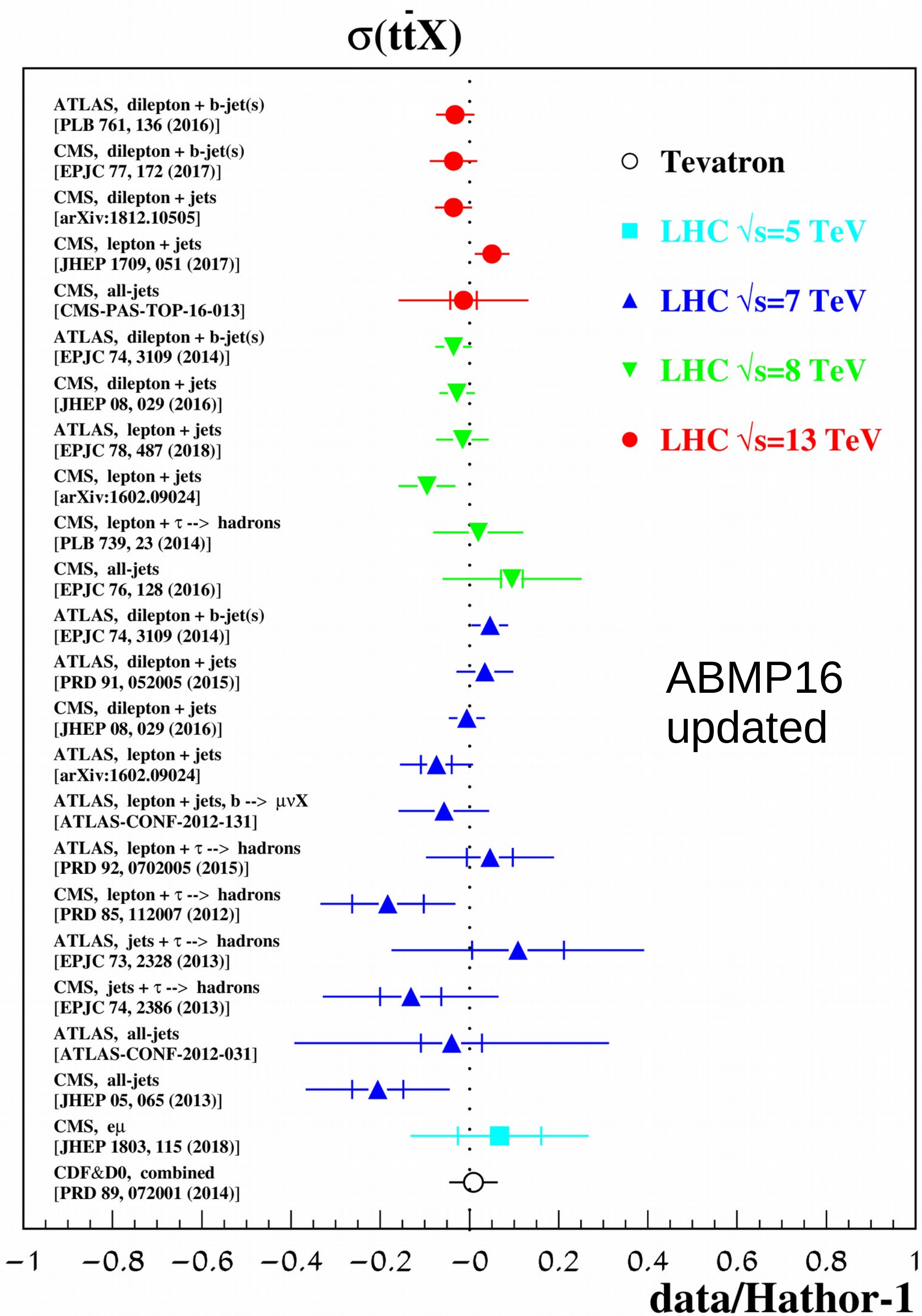

- Running t-quark mass is determined simultaneously with PDFs

$m_t(m_t)$= 160.9±1.1 GeV

m_t(pole)=170.4±1.2 GeV

m_t(MC)~172.5 GeV from LHC

m_t(pole)=170.5±0.8 GeV

CMS hep-ex/1904.05237

m_t(pole)=171.1±1.1 GeV

ATLAS hep-ex/1905.02302

(Hoang et al. try to quantify the difference between m_t(MC) and other determinations)

Hadronic charm production

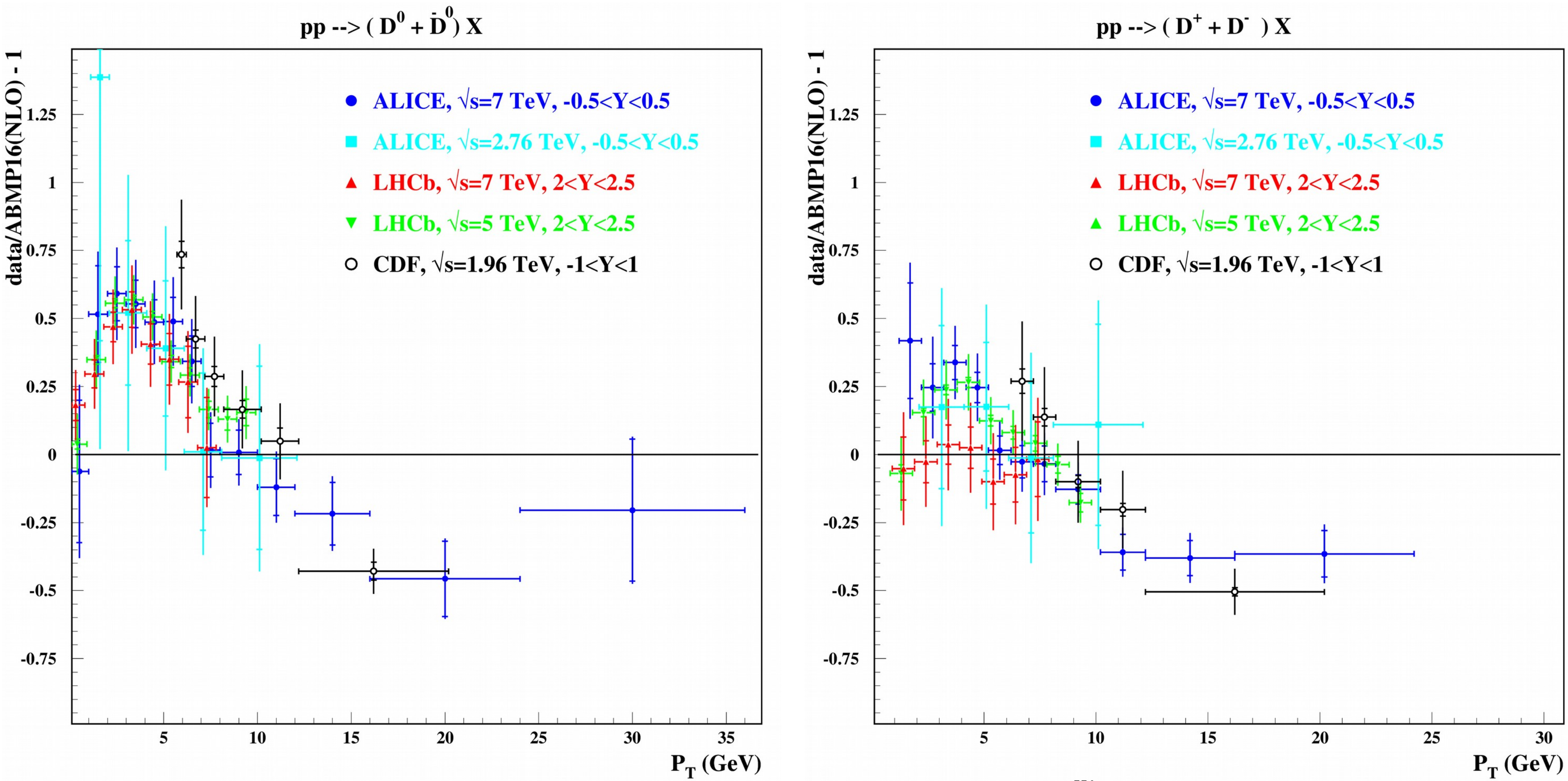

Theory: NLO QCD + hadronization (PYTHIA)

Garzelli , DIS2019

- Two-particle decay data provide more consistent picture
- The shape of pulls cannot be improved by the PDF modification: Higher-order terms needed (and/or resummation)

Summary

- The FFN scheme provides nice agreement with existing HERA data on charm production; running c-quark mass

$$m_c(m_c)=1.250\pm0.019(\mathrm{exp.})-0.01(\mathrm{th.})\ \mathrm{GeV},$$

is in a good agreement with other determinations.

Enhanced small-x gluon is preferred by data; consistent with inclusive data, if stringent cut on Q^2 is imposed.

- Steady improvement in the quark PDFs' determination due to DY LHC data
  - disentangling d- and u-quark distributions at small x: negative isospin sea asymmetry at small x
  - improvement in the large-x d- and u-quark distributions: impact of the forward LHC and Tevatron data; however, no enhancement in d/u at large x is observed
  - somewhat enhanced strange distribution at small x; large-x enhancement reported by ATLAS seems to be an artifact of the PDF shape used
- NNLO corrections (with resummation) is needed for consistent use of the charm hadroproduction data

EXTRAS

NNLO tools benchmarking

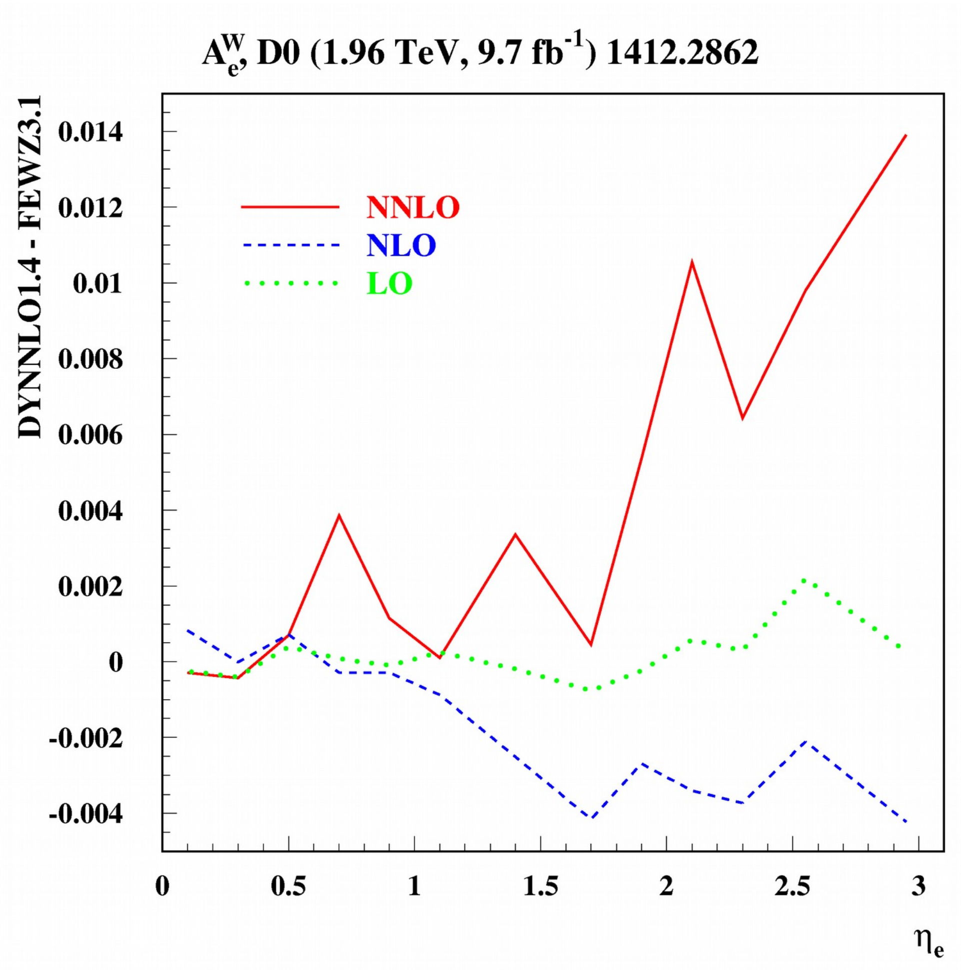

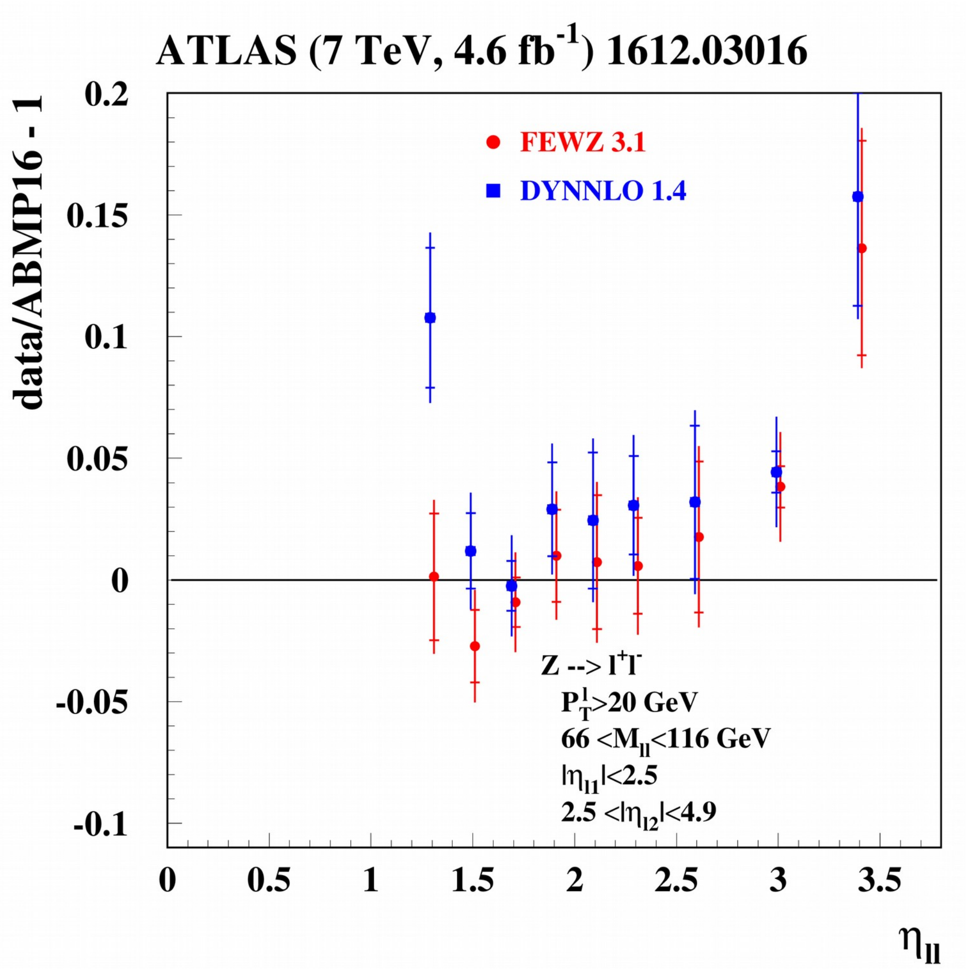

Yannick Ulrich, Barchelor thesis, Univ. of Hamburg 2015

DYNNLO-FEWZ difference not fully understood; further benchmarking is needed

Walker, this conference

TABLE II. The list of DIS and DY data used in the current analysis with the collider data listed first. The top-quark production data are detailed in Tables III and IV.

Experiment	Beam (E_b) or center-of-mass energy ($\sqrt{s}$)	$\mathcal{L}$ (1/fb)	Process	Kinematic cuts used in the present analysis (cf. orginal references for notations)	Ref.
			DIS		
HERA I + II	$\sqrt{s} = 0.225 \div 0.32$ TeV	0.5	$e^\pm p \to e^\pm X$	$2.5 \le Q^2 \le 50000$ GeV^2, $2.5 \times 10^{-5} \le x \le 0.65$	[4]
			$e^\pm p \to \overset{(-)}{\nu} X$	$200 \le Q^2 \le 50000$ GeV^2, $1.3 \times 10^{-2} \le x \le 0.40$	
BCDMS	$E_b = 100 \div 280$ GeV		$\mu^+ p \to \mu^+ X$	$7 < Q^2 < 230$ GeV^2, $0.07 \le x \le 0.75$	[61]
NMC	$E_b = 90 \div 280$ GeV		$\mu^+ p \to \mu^+ X$	$2.5 \le Q^2 < 65$ GeV^2, $0.009 \le x < 0.5$	[60]
SLAC-49a	$E_b = 7 \div 20$ GeV		$e^- p \to e^- X$	$2.5 \le Q^2 < 8$ GeV^2, $0.1 < x < 0.8$, $W \ge 1.8$ GeV	[54] [62]
SLAC-49b	$E_b = 4.5 \div 18$ GeV		$e^- p \to e^- X$	$2.5 \le Q^2 < 20$ GeV^2, $0.1 < x < 0.9$, $W \ge 1.8$ GeV	[54] [62]
SLAC-87	$E_b = 8.7 \div 20$ GeV		$e^- p \to e^- X$	$2.5 \le Q^2 < 20$ GeV^2, $0.3 < x < 0.9$, $W \ge 1.8$ GeV	[54] [62]
SLAC-89b	$E_b = 6.5 \div 19.5$ GeV		$e^- p \to e^- X$	$2.5 \le Q^2 \le 19$ GeV^2, $0.17 < x < 0.9$, $W \ge 1.8$ GeV	[56] [62]
			DIS heavy-quark production		
HERA I + II	$\sqrt{s} = 0.32$ TeV		$e^\pm p \to e^\pm c X$	$2.5 \le Q^2 \le 2000$ GeV^2, $2.5 \times 10^{-5} \le x \le 0.05$	[63]
H1	$\sqrt{s} = 0.32$ TeV	0.189	$e^\pm p \to e^\pm b X$	$5 \le Q^2 \le 2000$ GeV^2, $2 \times 10^{-4} \le x \le 0.05$	[15]
ZEUS	$\sqrt{s} = 0.32$ TeV	0.354	$e^\pm p \to e^\pm b X$	$6.5 \le Q^2 \le 600$ GeV^2, $1.5 \times 10^{-4} \le x \le 0.035$	[16]
CCFR	$87 \lesssim E_b \lesssim 333$ GeV		$\overset{(-)}{\nu} N \to \mu^\pm c X$	$1 \le Q^2 < 170$ GeV^2, $0.015 \le x \le 0.33$	[64]
CHORUS	$\langle E_b \rangle \approx 27$ GeV		$\nu N \to \mu^+ c X$		[18]
NOMAD	$6 \le E_b \le 300$ GeV		$\nu N \to \mu^+ c X$	$1 \le Q^2 < 20$ GeV^2, $0.02 \lesssim x \le 0.75$	[17]
NuTeV	$79 \lesssim E_b \lesssim 245$ GeV		$\overset{(-)}{\nu} N \to \mu^\pm c X$	$1 \le Q^2 < 120$ GeV^2, $0.015 \le x \le 0.33$	[64]
			DY		
ATLAS	$\sqrt{s} = 7$ TeV	0.035	$pp \to W^\pm X \to l^\pm \nu X$	$p_T^l > 20$ GeV, $p_T^\nu > 25$ GeV, $m_T > 40$ GeV	[67]
			$pp \to ZX \to l^+ l^- X$	$p_T^l > 20$ GeV, $66 < m_{ll} < 116$ GeV	
	$\sqrt{s} = 13$ TeV	0.081	$pp \to W^\pm X \to l^\pm \nu X$	$p_T^\nu > 25$ GeV, $m_T > 50$ GeV	[26]
			$pp \to ZX \to l^+ l^- X$	$p_T^l > 25$ GeV, $66 < m_{ll} < 116$ GeV	
CMS	$\sqrt{s} = 7$ TeV	4.7	$pp \to W^\pm X \to \mu^\pm \nu X$	$p_T^\mu > 25$ GeV	[24]
	$\sqrt{s} = 8$ TeV	18.8	$pp \to W^\pm X \to \mu^\pm \nu X$	$p_T^\mu > 25$ GeV	[25]
DØ	$\sqrt{s} = 1.96$ TeV	7.3	$\bar{p}p \to W^\pm X \to \mu^\pm \nu X$	$p_T^\mu > 25$ GeV, $E\!\!\!/_T > 25$ GeV	[23]
		9.7	$\bar{p}p \to W^\pm X \to e^\pm \nu X$	$p_T^e > 25$ GeV, $E\!\!\!/_T > 25$ GeV	[22]
LHCb	$\sqrt{s} = 7$ TeV	1	$pp \to W^\pm X \to \mu^\pm \nu X$	$p_T^\mu > 20$ GeV	[19]
			$pp \to ZX \to \mu^+ \mu^- X$	$p_T^\mu > 20$ GeV, $60 < m_{\mu\mu} < 120$ GeV	
	$\sqrt{s} = 8$ TeV	2	$pp \to ZX \to e^+ e^- X$	$p_T^e > 20$ GeV, $60 < m_{ee} < 120$ GeV	[21]
		2.9	$pp \to W^\pm X \to \mu^\pm \nu X$	$p_T^\mu > 20$ GeV	[20]
			$pp \to ZX \to \mu^+ \mu^- X$	$p_T^\mu > 20$ GeV, $60 < m_{\mu\mu} < 120$ GeV	
FNAL-605	$E_b = 800$ GeV		$pCu \to \mu^+ \mu^- X$	$7 \le M_{\mu\mu} \le 18$ GeV	[68]
FNAL-866	$E_b = 800$ GeV		$pp \to \mu^+ \mu^- X$	$4.6 \le M_{\mu\mu} \le 12.9$ GeV	[69]
			$pD \to \mu^+ \mu^- X$		

TABLE III. The data on the $t\bar{t}$-production cross section from the LHC used in the present analysis. The errors given are combinations of the statistical and systematic ones. An additional error of 1.4, 3.3, 4.2 and 12 pb due to the beam energy uncertainty applies to all entries for the collision energy of $\sqrt{s} = 5$, 7, 8 and 13 TeV, respectively. The quoted values are rounded for the purpose of a compact presentation.

		Cross section (pb)						
$\sqrt{s}$ (TeV)		5	7		8		13	
Experiment		CMS	ATLAS	CMS	ATLAS	CMS	ATLAS	CMS
Decay mode	dilepton + b-jet(s)		183 ± 6 [36]		243 ± 8 [36]		818 ± 36 [37]	792 ± 43 [38]
	dilepton + jets		181 ± 11 [33]	174 ± 6 [34]		245 ± 9 [34]		746 ± 86 [35]
	lepton + jets			162 ± 14 [39]	260 ± 24 [40]	229 ± 15 [39]		836 ± 133 [41]
	lepton + jets, $b \to \mu\nu X$		165 ± 38 [42]					
	lepton + $\tau \to$ hadrons		183 ± 25 [43]	143 ± 26 [44]		257 ± 25 [51]		
	jets + $\tau \to$ hadrons		194 ± 49 [46]	152 ± 34 [47]				
	all-jets		168 ± 60 [48]	139 ± 28 [49]		276 ± 39 [45]		834^{+123}_{-109} [50]
	eμ	82 ± 23 [52]						

TABLE IV. The data on single-top production in association with a light quark q or $\bar{b}$-quark from the LHC and Tevatron used in the present analysis. The errors given are combinations of the statistical, systematic, and luminosity ones.

Experiment	ATLAS			CMS			CDF&DØ
$\sqrt{s}$ (TeV)	7	8	13	7	8	13	1.96
Final states	tq	tq	tq	tq	tq	tq	$tq, t\bar{b}$
Reference	[27]	[28]	[29]	[30]	[31]	[32]	[53]
Luminosity (1/fb)	4.59	20.3	3.2	2.73	19.7	2.3	9.7×2
Cross section (pb)	68 ± 8	82.6 ± 12.1	247 ± 46	67.2 ± 6.1	83.6 ± 7.7	232 ± 30.9	$3.30^{+0.52}_{-0.40}$ (sum)

Impact of high twists on SLAC data

sa, Blümlein, Moch PRD 86, 054009 (2012)

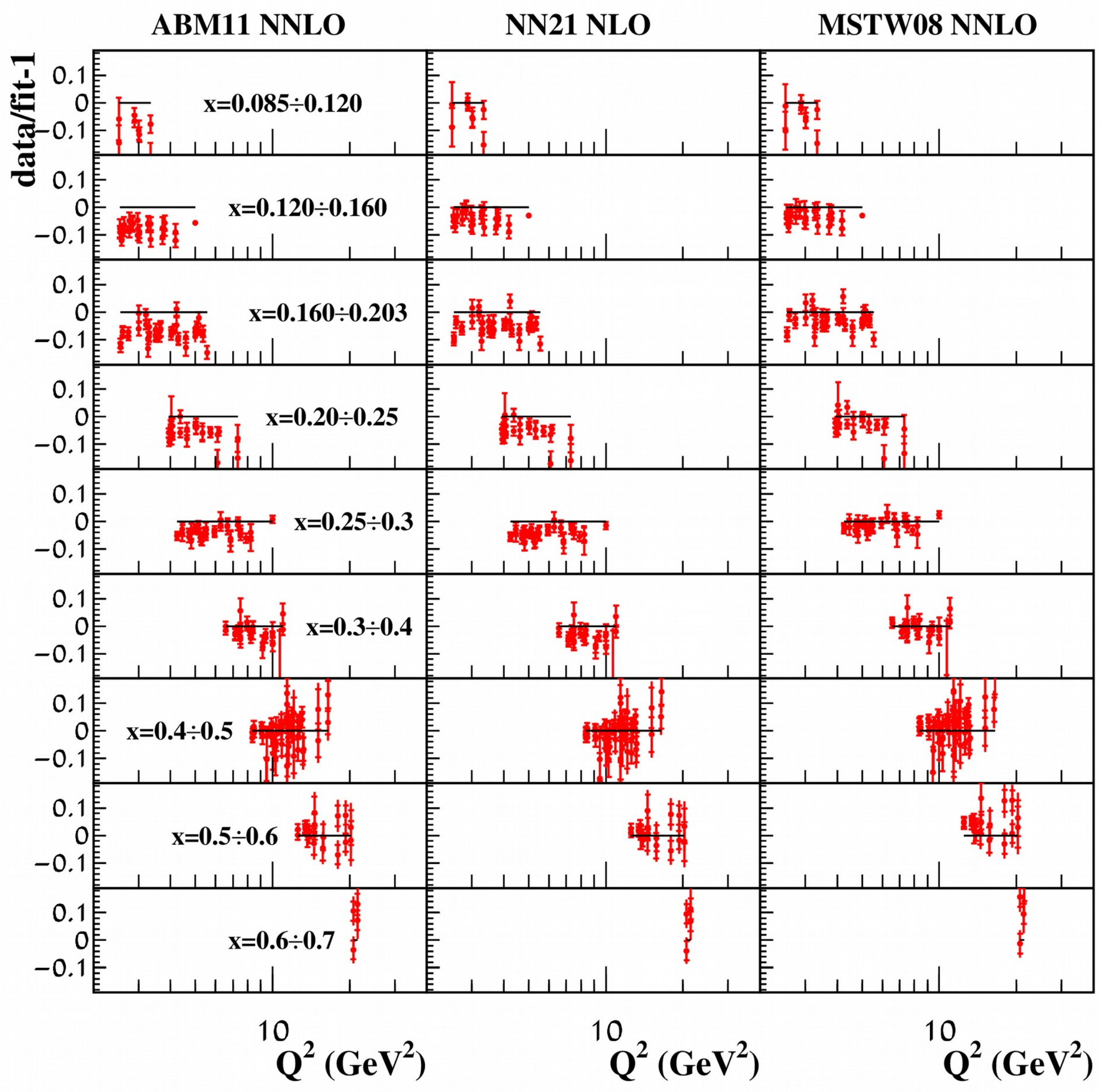

Power-like terms affect comparison even with a “safe” cut $W^2 \geq 12.5$ GeV^2

Checking styles of PDF shape

	ABMP16	CJ15	CT10	CT14	epWZ16	MMHT14
N_{PDF}	28	21	26	26	14	31
μ_0^2 (GeV^2)	9	1.69	1.69	1.69	1.9	1
χ^2	4065	4108	4148	4153	4336	4048
PDF shape	$x^\alpha(1-x)^\beta$ $\exp[P(x,\ln(x))]$	$x^\alpha(1-x)^\beta P(x,\sqrt{x})$	$x^\alpha(1-x)^\beta$ $\exp[P(x,\sqrt{x})]$	$x^\alpha(1-x)^\beta$ $\exp[P(x,\sqrt{x})]$	$x^\alpha(1-x)^\beta P(x,\sqrt{x})$	$x^\alpha(1-x)^\beta P(x,\sqrt{x})$
Constraints		$\bar{u}=\bar{d}$ $(x\to 0)$	$\alpha_{uv}=\alpha_{dv}$ $\alpha_{\bar{u}}=\alpha_{\bar{d}}=\alpha_s$ $\bar{u}=\bar{d}$ $(x\to 0)$	$\alpha_{uv}=\alpha_{dv}$ $\beta_{uv}=\beta_{dv}$ $\alpha_{\bar{u}}=\alpha_{\bar{d}}=\alpha_s$	$\alpha_{\bar{u}}=\alpha_{\bar{d}}=\alpha_s$ $\bar{u}=\bar{d}$ $(x\to 0)$	
$\alpha_s(M_Z)$	0.1153	0.1147	0.1150	0.1160	0.1162	0.1158

- Various PDF-shape modifications provide comparable description with N_{PDF}~30
- Some deterioration, which happens in cases is apparently due to constraints on large(small)-x exponents

Conservative estimate of uncertainty in $\alpha_s(M_Z)$: 0.0007, more optimistic: 0.0003

Electroweak vacuum stability

$$m_H = 129.6\,\mathrm{GeV} + 1.8\times\left(\frac{m_t^{\mathrm{pole}} - 173.34\ \mathrm{GeV}}{0.9}\right) - 0.5\times\left(\frac{\alpha_s^{(n_f=5)}(M_Z) - 0.1184}{0.0007}\right)\mathrm{GeV} \pm 0.3\ \mathrm{GeV}\,,$$

Buttazzo et al., JHEP 12, 089 (2013)

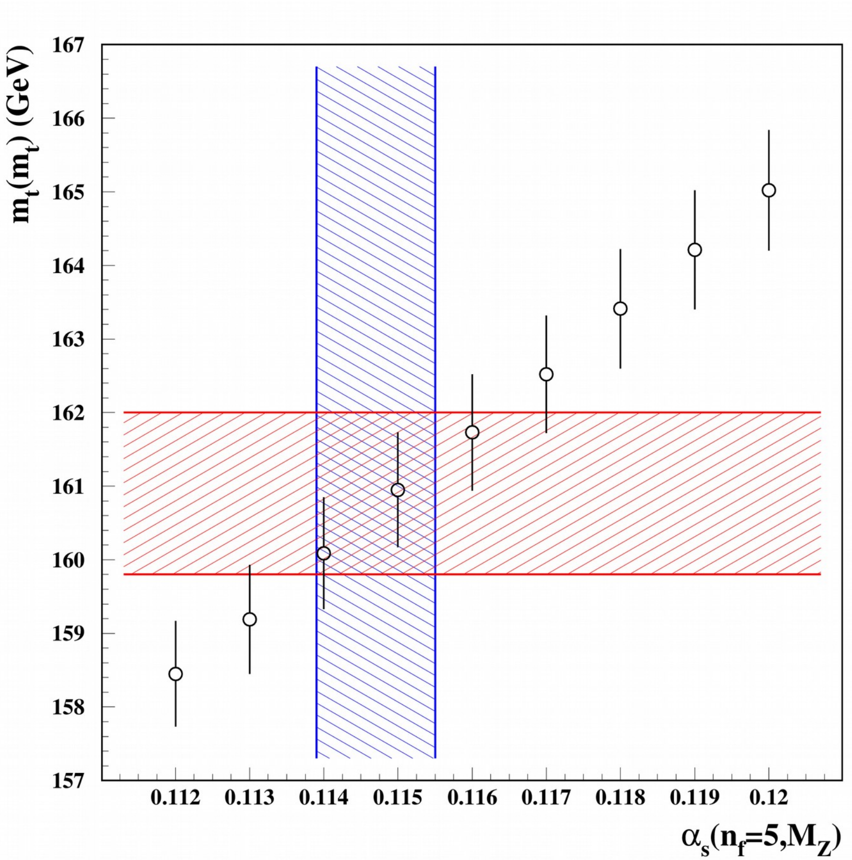

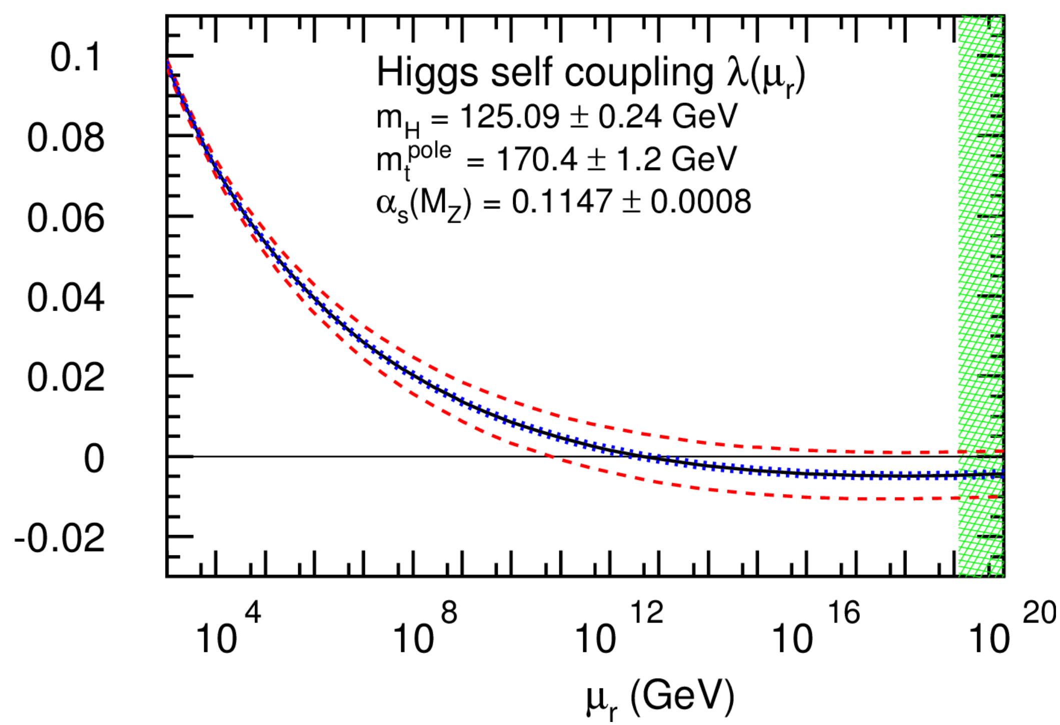

mr: **Kniehl, Pikelner, Veretin CPC 206, 84 (2016)**

Vacuum stability is quite sensitive to the t-quark mass; stability is provided up to Plank-mass scale using α_s and m_t in a consistent way.

t-quark: single production (mass determination)

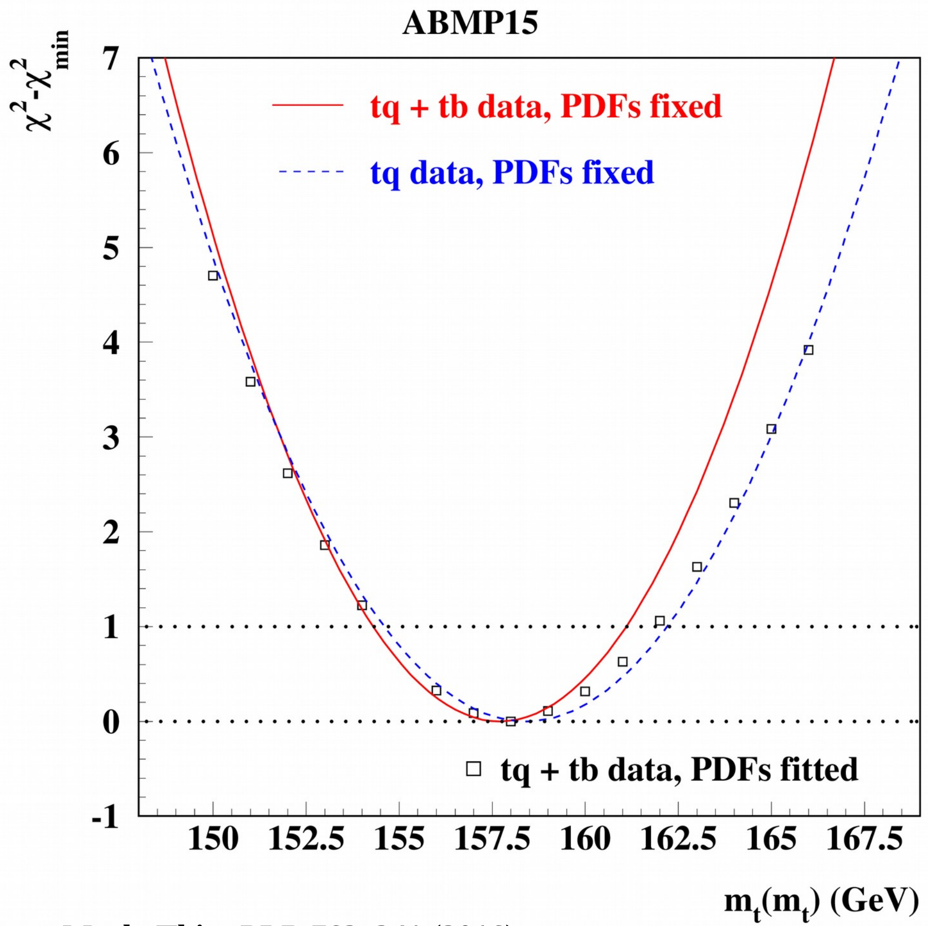

sa, Moch, Thier PLB 763, 341 (2016)

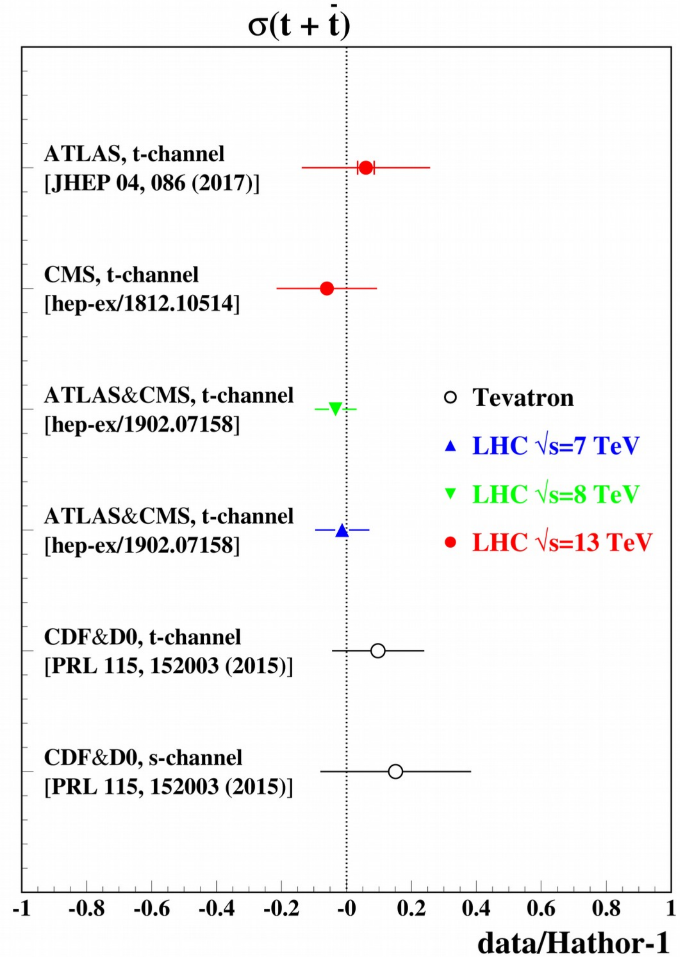

$m_t(m_t)$= 161.1± 3.8GeV (single-top only)

Channel	ABM12 [21]	ABMP15 [52]	CT14 [55]	MMHT14 [56]	NNPDF3.0 [57]
$t\bar{t}$	158.6 ± 0.6	158.4 ± 0.6	164.7 ± 0.6	164.6 ± 0.6	164.3 ± 0.6
t-channel	158.7 ± 3.7	158.0 ± 3.7	160.1 ± 3.8	160.5 ± 3.8	164.0 ± 3.8
s- & t-channel	158.4 ± 3.3	157.7 ± 3.3	159.1 ± 3.4	159.6 ± 3.4	162.4 ± 3.5

Impact of the t-quark data on the ABMP16 fit

MSbar

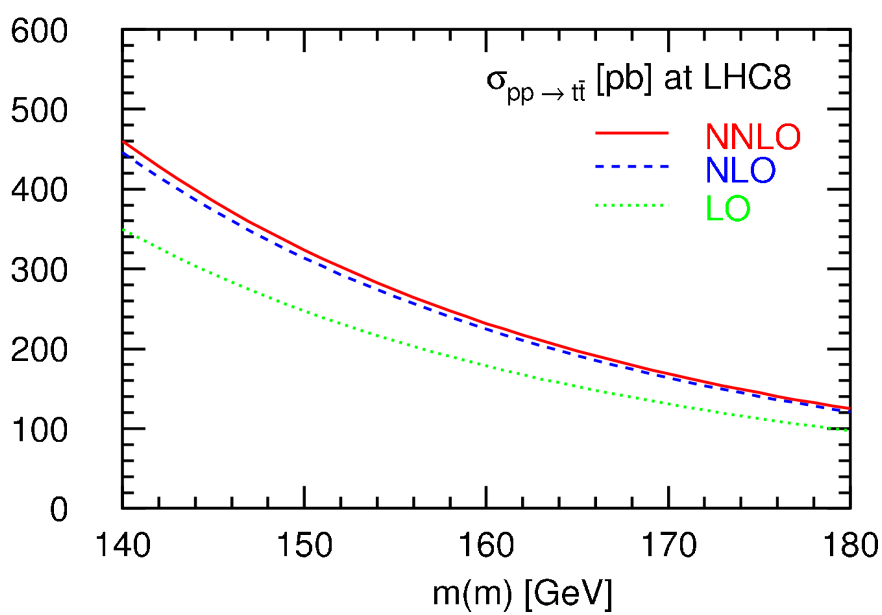

Pole

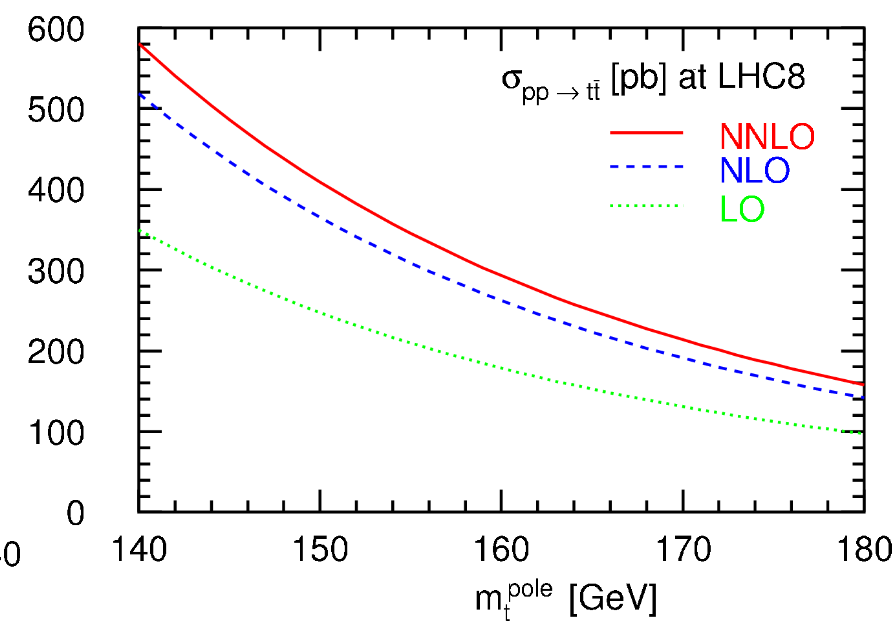

HATHOR (NNLO terms are checked with TOP++)

Langenfeld, Moch, Uwer PRD 80, 054009 (2009)

Running mass definition provides nice perturbative stab

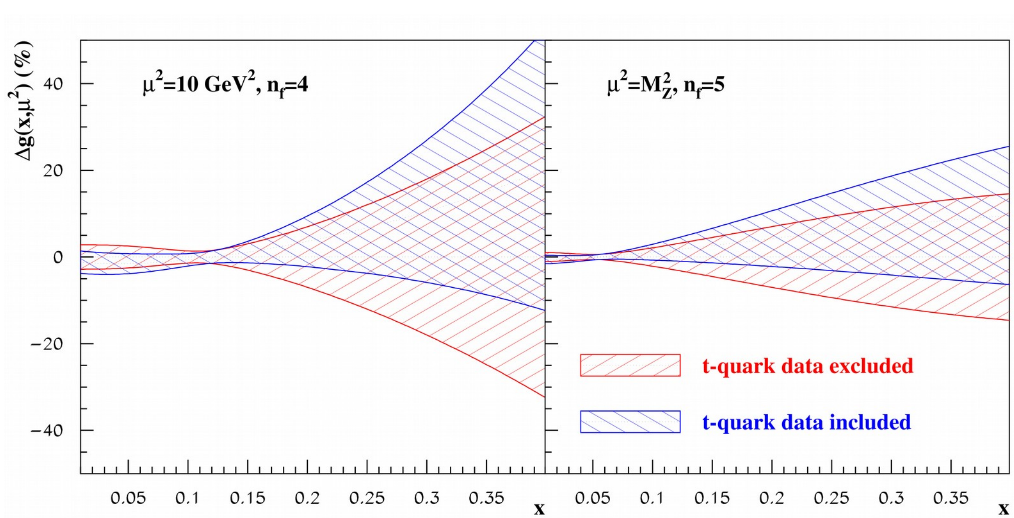

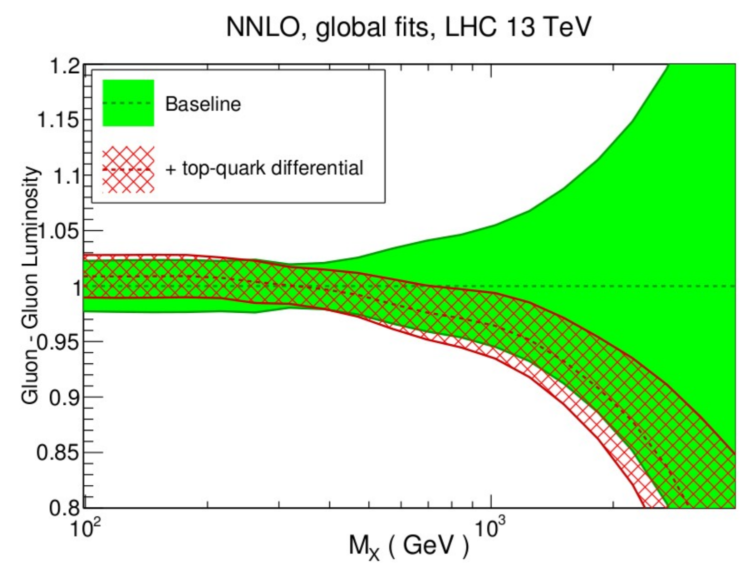

Czakon et al., JHEP 1704, 044 (2017)

fastNLO

HERA charm data and $m_c(m_c)$

H1/ZEUS ZPC 73, 2311 (2013)

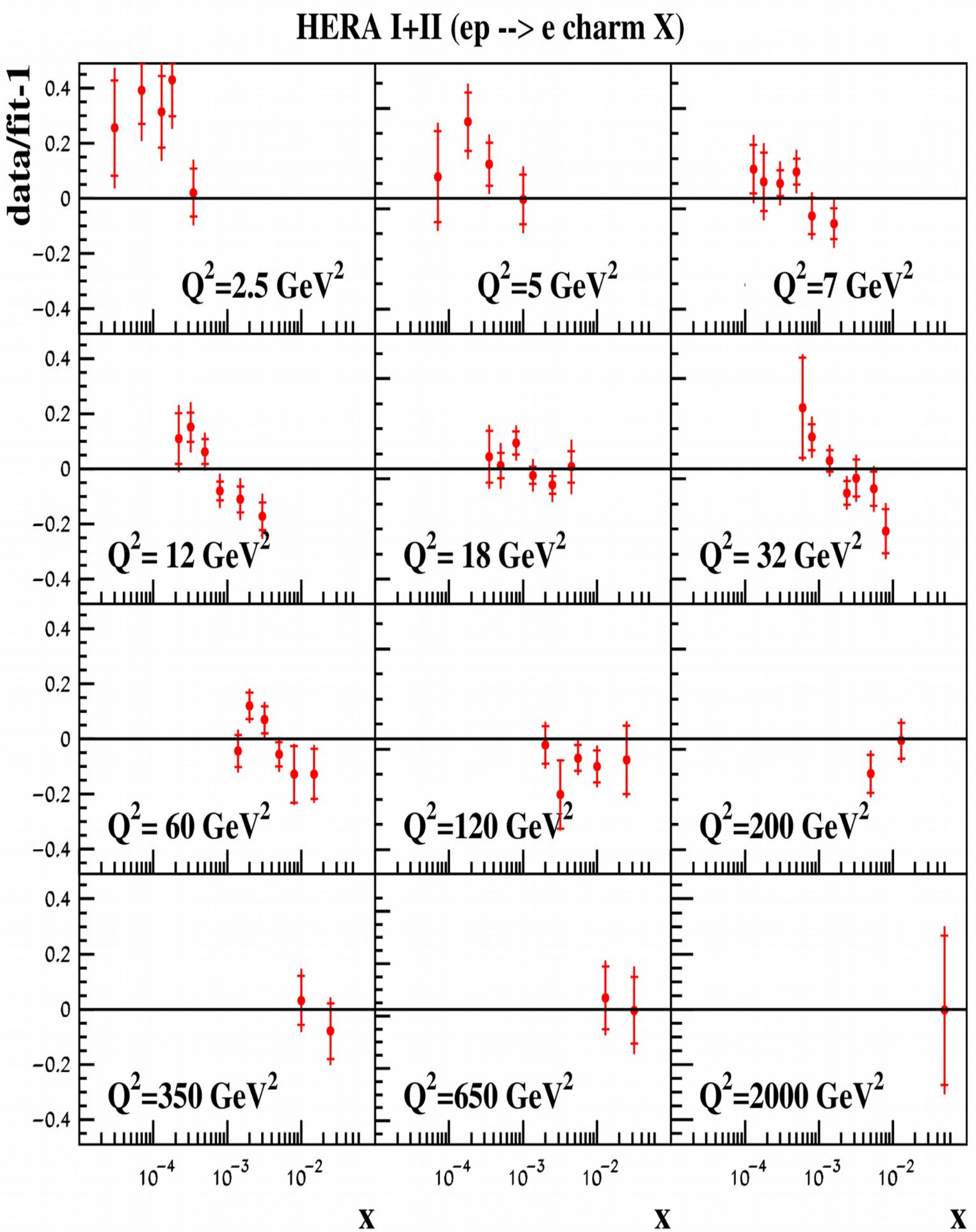

$m_c(m_c)$=1.246±0.023 (h.o.) GeV NNLO

Kiyo, Mishima, Sumino PLB 752, 122 (2016)

X^2/NDP=66/52
$m_c(m_c)$=1.252±0.018(exp.)-0.01(th.) GeV ABMP16

$m_c(m_c)$=1.24±0.03(exp.) GeV ABM12

m_c(pole)~1.9 GeV (NNLO)

Marquard et al. PRL 114, 142002 (2015)

- RT optimal
  X^2/NDP=82/52 NNLO
  m_c(pole)=1.25 GeV MMHT14 EPJC 75, 204 (2015)
- S-ACOT-χ
  X^2/NDP=59/47 NNLO
  m_c(pole)=1.3 GeV CT14 PRD 93, 033006 (2016)
- F0NLL
  X^2/NDP=60/47 NNLO
  m_c(pole)=1.275 GeV NNPDF3.0 JHEP 504, 040 (2015)
- F0NLL
  X^2/NDP=54/37 NNLO
  m_c(pole)=1.51 GeV, intrinsic charm included

NNPDF3.1 hep-ph/1706.00428

Accardi, et al. EPJC 76, 471 (2016)

Higher twists: fit with stringent cut on Q,W

χ^2/NDP

	HT fitted $Q^2>2.5\ GeV^2$, $W>1.8$ GeV	HT=0, $Q^2>10\ GeV^2$, $W^2>12.5\ GeV^2$
HERA	1510/1168	1220/1007
Fixed target: SLAC, NMC,BCDMS	1145/1008	498/444

Value of χ^2 is stable w.r.t. to cuts

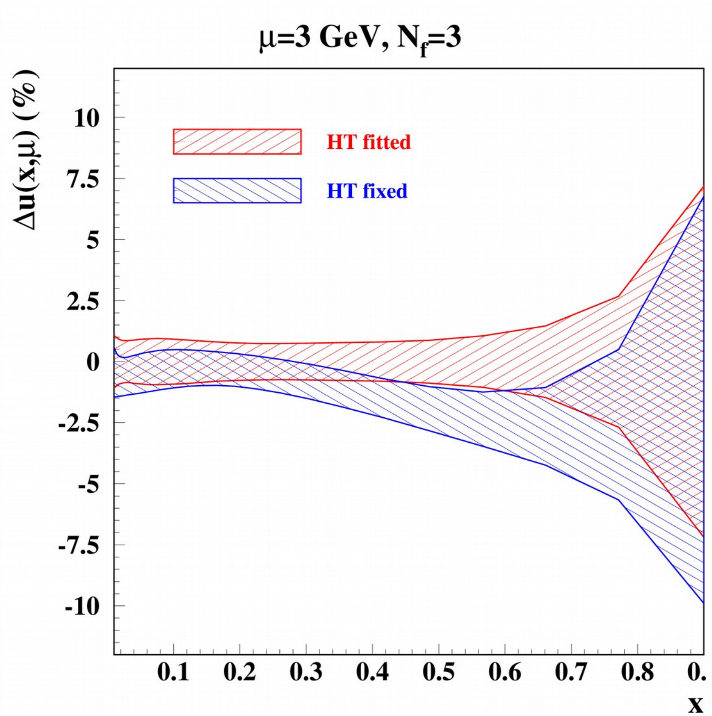

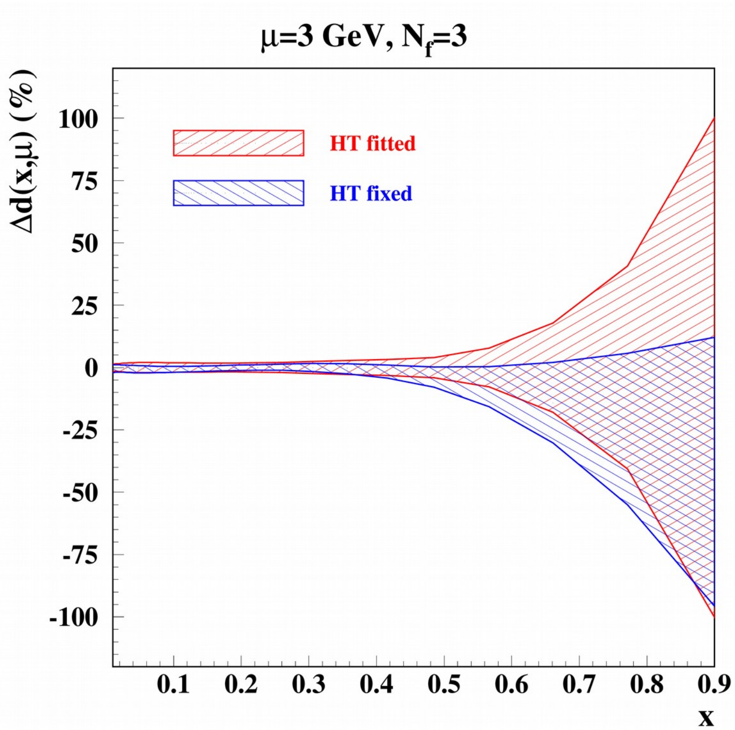

Stringent cut affects high-x data, however, the large-x PDF uncertainties remain stable

Strange sea from the νN DIS

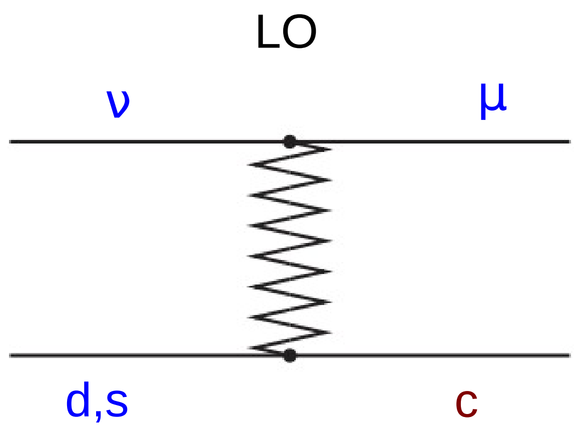

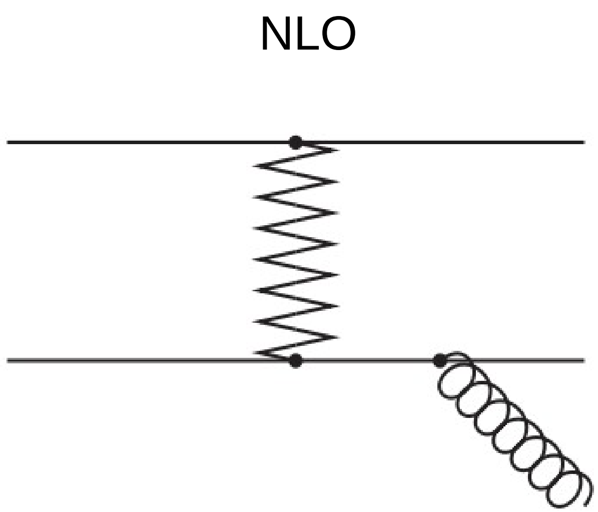

Two decay modes of c-quark are used: hadronic (emulsion experiments) and semi-leptonic (electronic experiments)

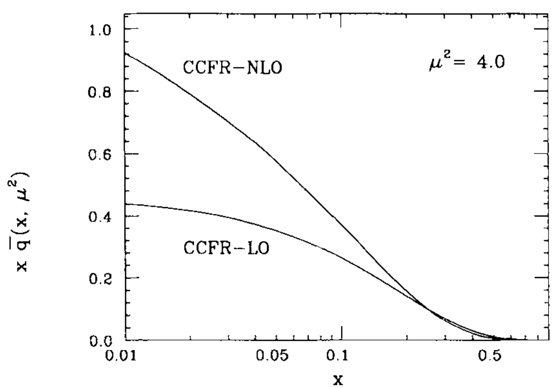

Fig. 3. The quark sea distribution $x\bar{q}(x, \mu^2 = 4.0\,\mathrm{GeV}^2/\mathrm{c}^2)$ determined at next-to-leading order and leading order

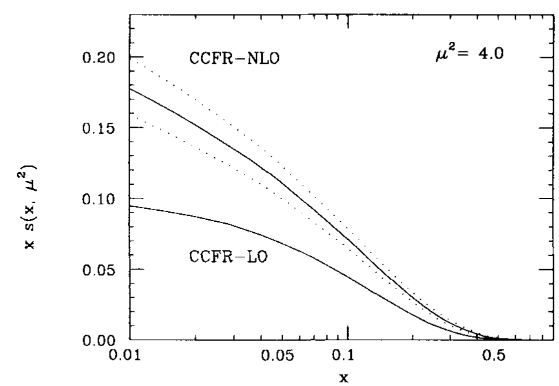

Fig. 4. The strange quark distribution $xs(x, \mu^2 = 4.0\,\mathrm{GeV}^2/\mathrm{c}^2)$ determined at next-to-leading order (described in section 4.1) and leading order. The band around the NLO curve indicates the $\pm 1\sigma$ uncertainty in the distribution

CCFR ZPC 65, 189 (1995)

Primary source for the strange sea was for a long time neutrino-induced charm production measured by CCFR/NuTeV at Fermilab preferring a suppression of ~0.5 w.r.t. non-strange sea

NuTeV/CCFR data in the PDF fit framework

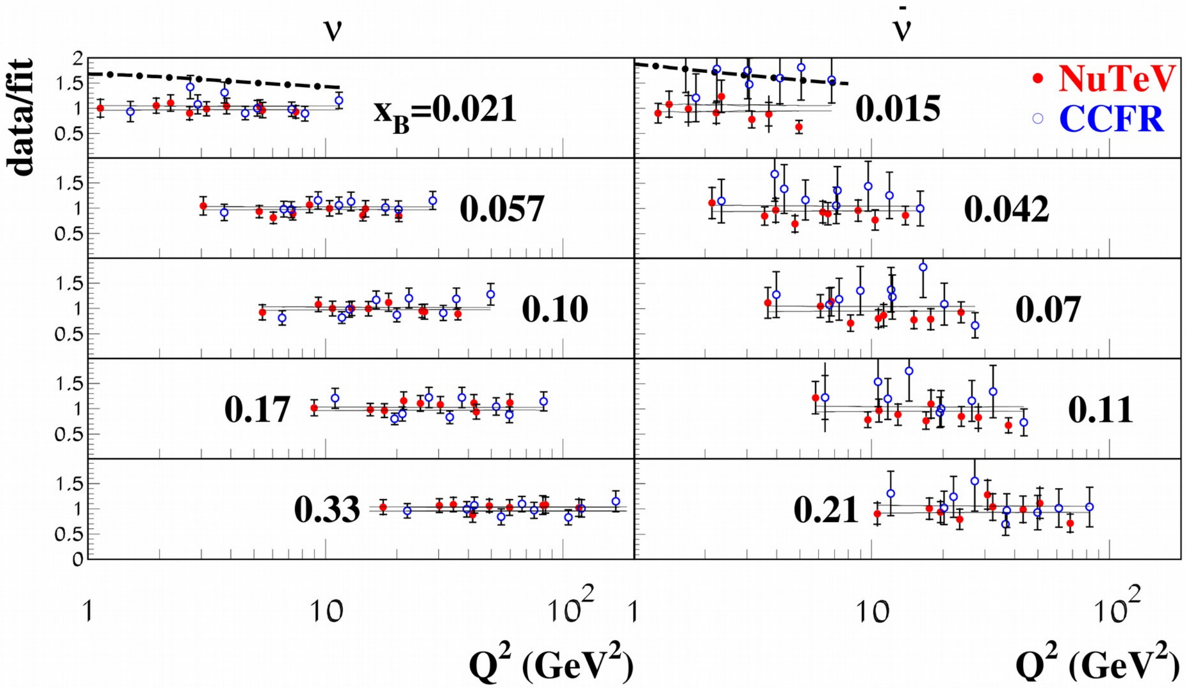

- CCFR and NuTeV are in a good agreement
- Charge asymmetry in the strange sea is consistent with 0 within uncertainties

sa, Kulagin, Petti PLB 675, 433 (2009)

$$\kappa_s(\mu^2) = \frac{\int_0^1 x[s(x,\mu^2) + \bar{s}(x,\mu^2)]dx}{\int_0^1 x[\bar{u}(x,\mu^2) + \bar{d}(x,\mu^2)]dx},$$

Integral suppression factor K_s(20 GeV^2)=0.62±0.04 is obtained

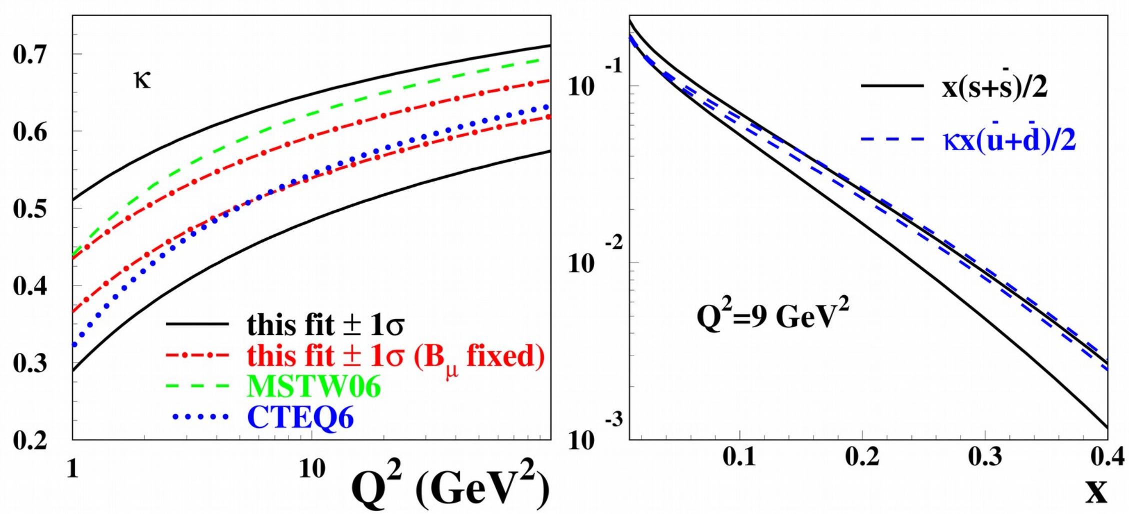

NOMAD charm data

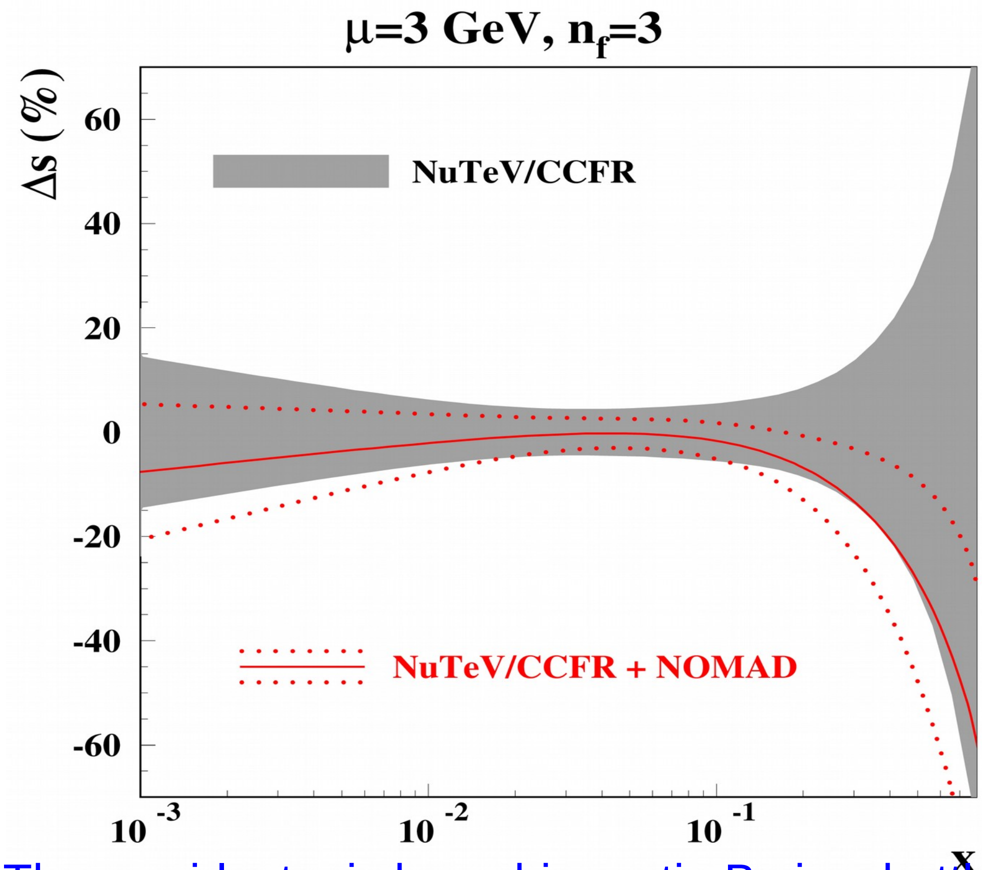

NOMAD NPB 876, 339 (2013)

- The data on ratio 2μ/incl. CC ratio with the 2μ statistics of 15000 events (much bigger than in earlier CCFR and NuTeV samples).
- Systematics, nuclear corrections, etc. cancel in the ratio
- Pull down strange quarks at x>0.1 with a sizable uncertainty reduction

The semi-leptonic branching ratio B_μ is a bottleneck

– weighted average of the charmed-hadron rates

$$B_\mu(E_\nu)=\sum_h r^h(E_\nu)B^h_\mu = a/(1+b/E_\nu)$$

– fitted simultaneously with the PDFs, etc. using the constraint from the emulsion data

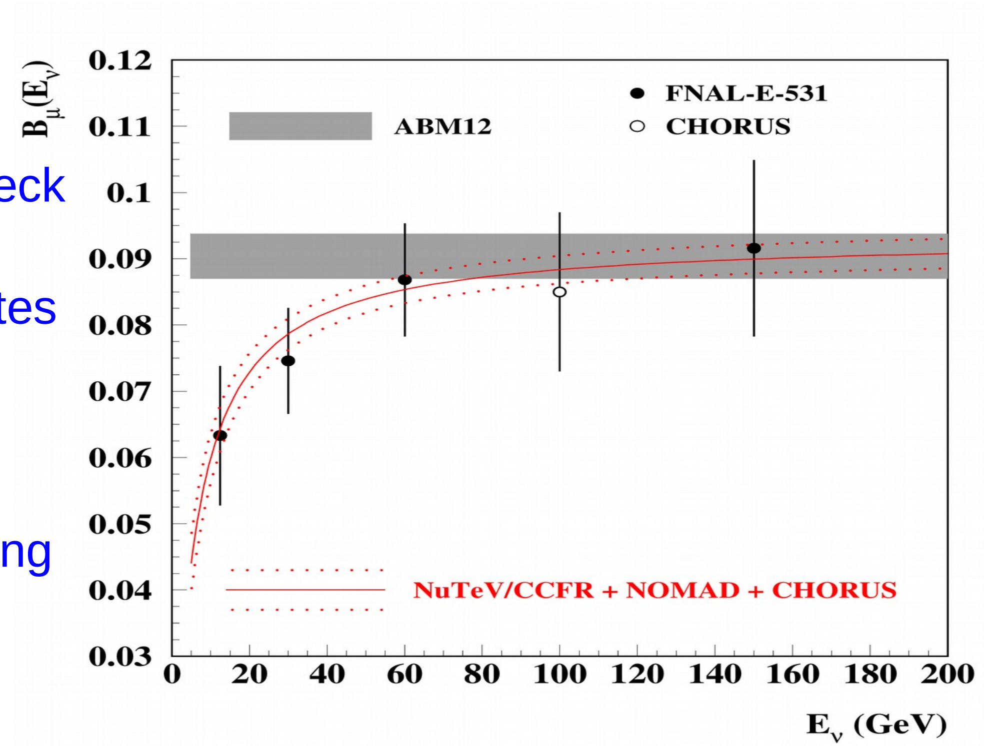

ATLAS strange enhancement

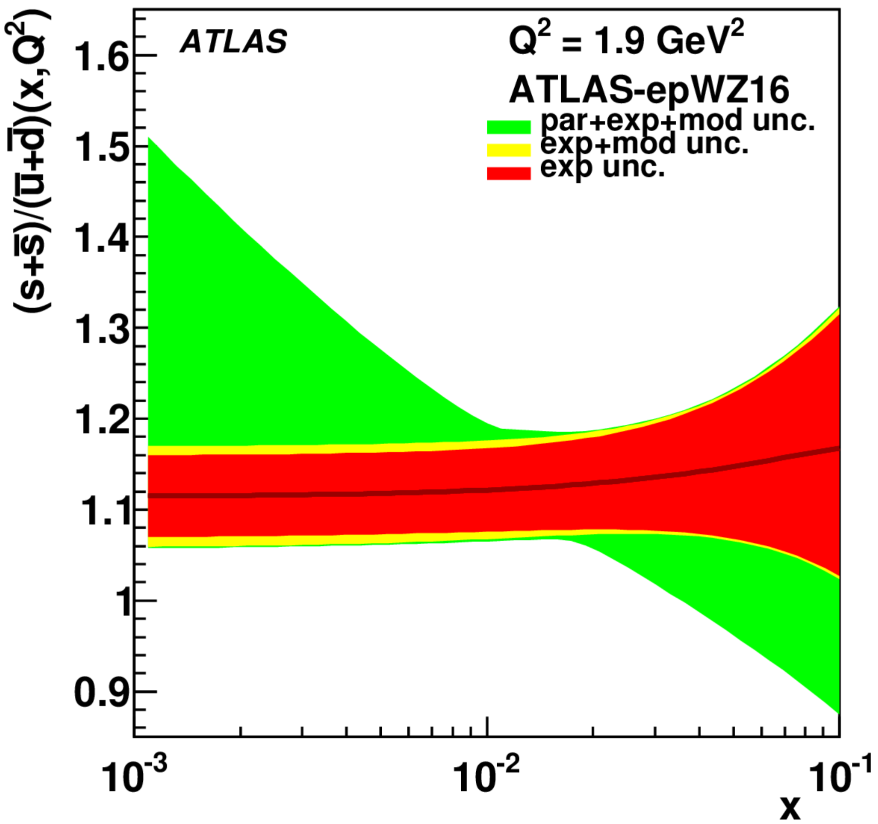

ATLAS arXiv:1612.03016

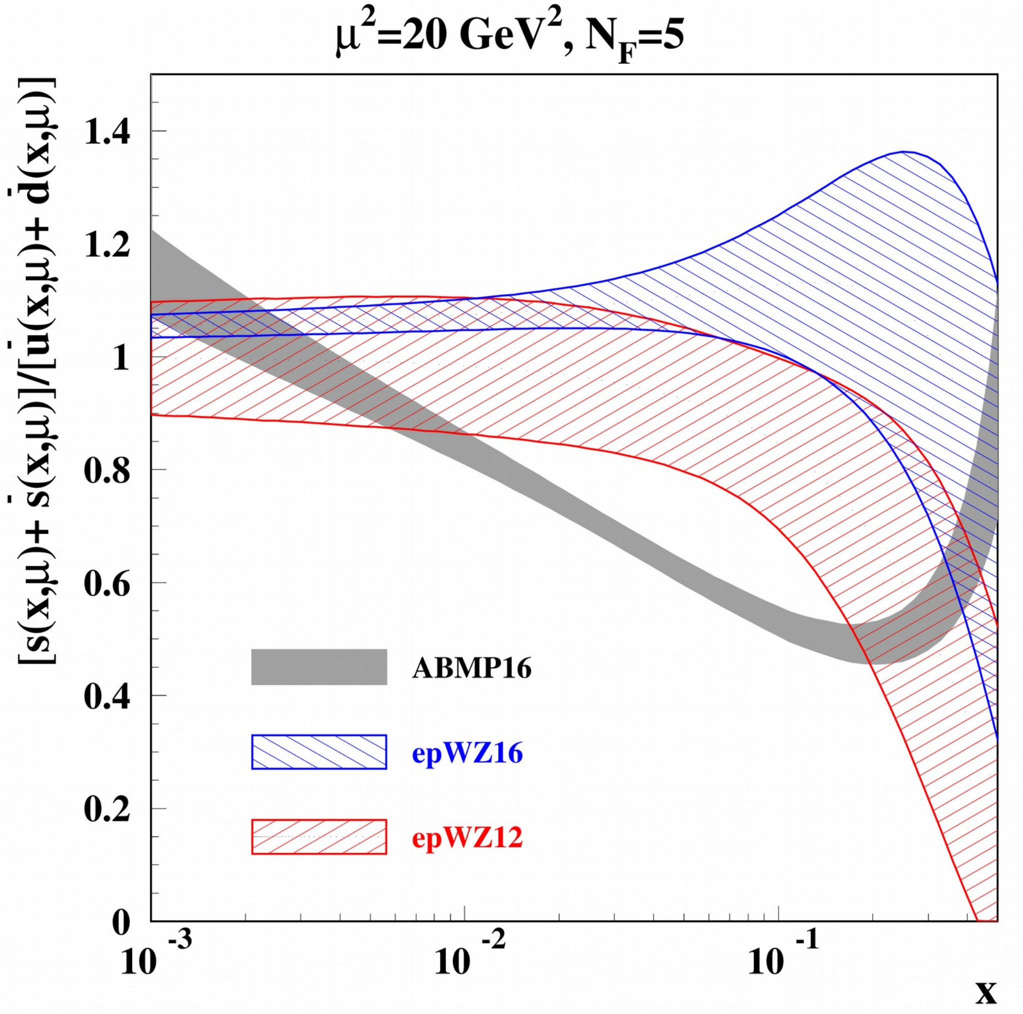

The epWZ16 strange-sea determined from analysis of the combined HERA-ATLAS data is enhanced as compared to other (earlier) determinations

ABM strange sea determination is in particular based on the dimuon neutrino-nucleon DIS production (NuTeV/CCFR and NOMAD) that gives a strange sea suppression ~0.5 at x~0.2

- *Disentangling d- and s- contribution?*
- *Impact of the nuclear corrections?*
- *.....?*

Intrinsic charm: pitfalls

- **No mass singularities** for massive partons ⇒ collinear QCD evolution does not work
- The mass singularities $\sim\ln(\mu/m_h)$ appear at $\mu \gg m_h$ and the evolution restores. New charm(bottom) quark distribution may be introduced, however, extrapolation to smaller scales is still problematic
- Intrinsic charm is often introduced within the VFN framework ⇒ interplay with the "standard" VFN modeling of power-like terms
- Original formulation of the intrinsic charm implies its power-like behavior;

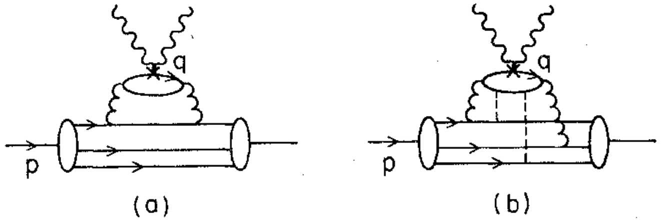

FIG. 7. (a) Example with contribution to the deep-inelastic structure functions from an extrinsic quark q; (b) from an intrinsic quark q.

Brodsky, Peterson, Sakai PRD 23, 2745 (1981)

- Strong constraint on such terms was obtained from analysis of the DIS inclusive and semi-inclusive data

Jimenez-Delgado, Hobbs, Londergan, Melnitchouk PRL 114, 082002 (2015)

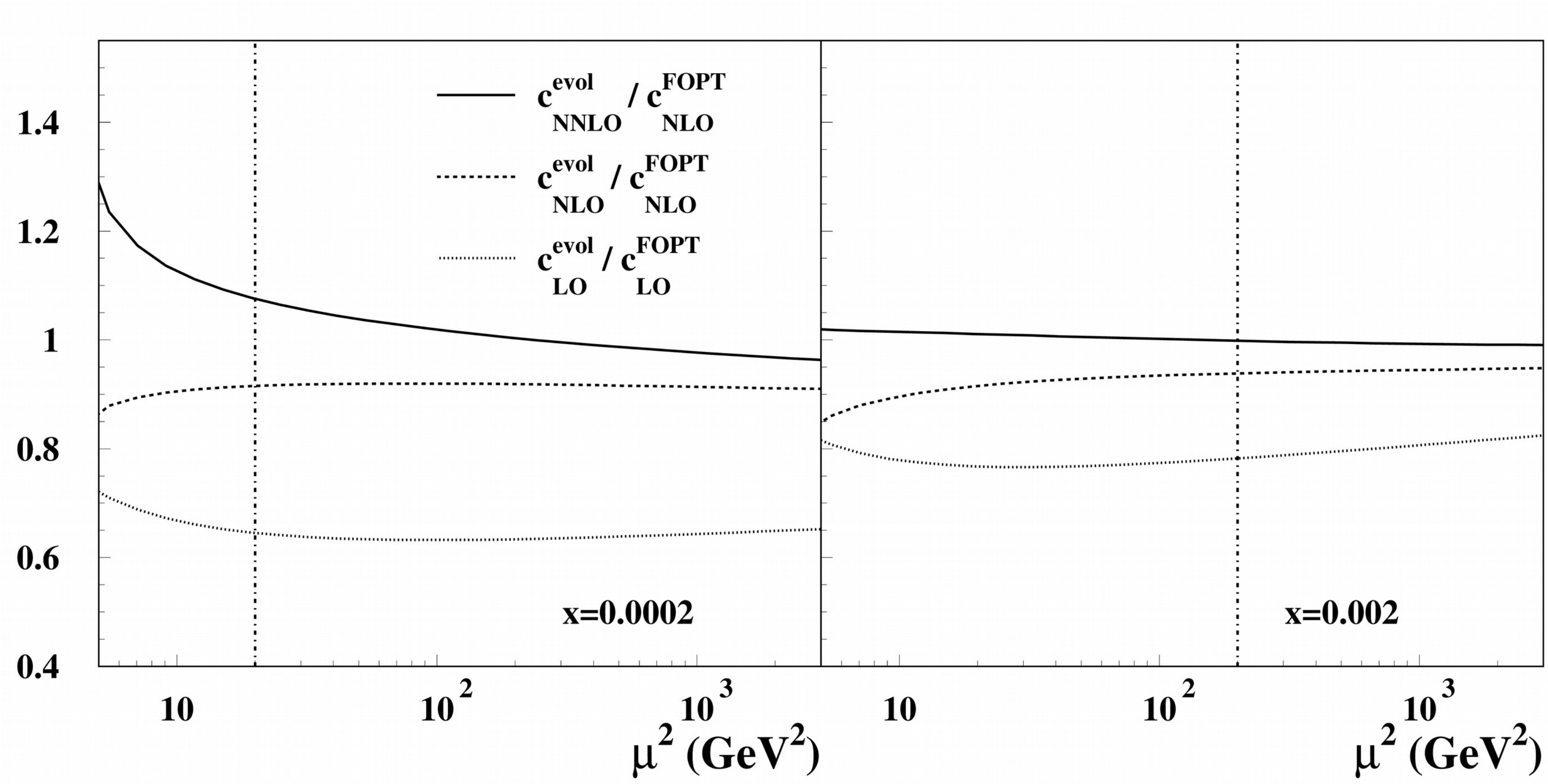

$c^{evol}_{NNLO} / c^{FOPT}_{NLO}$
$c^{evol}_{NLO} / c^{FOPT}_{NLO}$
$c^{evol}_{LO} / c^{FOPT}_{LO}$
1.4
1.2
1
0.8
0.6
0.4
x=0.0002
x=0.002
10
10^2
10^3
μ^2 (GeV^2)